A COMPARISON OF SURFACE MOISTURE BUDGET AND STRUCTURAL EQUATION MODELS IN HIGH LATITUDES: EVAPOTRANSPIRATION AND ATMOSPHERIC DRIVERS

By

Sarah M. Thunberg, B.S.

A Thesis Submitted in Partial Fulfillment of the Requirements

for the Degree of

Master of Science

in

Atmospheric Sciences

University of Alaska Fairbanks

August 2021

APPROVED:

John Walsh, Committee Co-Chair
Eugenie Euskirchen, Committee Co-Chair
Uma S. Bhatt, Committee Member
Javier Fochesatto, Department Chair
Department of Atmospheric Sciences
Kinchel C. Doerner, Dean
College of Natural Science and Mathematics
Richard Collins
Director of the Graduate School

Abstract

Arctic soil moisture is one of the most impactful and unknown aspects of the Arctic climate system. As the climate changes, surface soil moisture can impact water supplies, wildfire risk, and vegetation stress, all of which have consequences for terrestrial ecosystems and human activities. The present analysis is intended to (1) document seasonal and interannual variations of surface moisture fluxes in the Arctic region and (2) clarify the drivers of variations of net Precipitation minus Evapotranspiration (P-ET) across Arctic tundra and boreal vegetation and permafrost status. Forty-five flux tower sites were examined across boreal and tundra ecosystems across the Arctic and sub-arctic. The surface moisture budget at boreal forest sites in permafrost areas generally shows a moisture deficit in late spring and early summer, followed by a moisture surplus from late summer into autumn. The annual net P-ET is generally positive but can vary interannually by more than an order of magnitude. A factor analysis found the primary drivers of variations in evapotranspiration to be radiative fluxes, air temperature, and relative humidity, while a path analysis found windspeed to have the largest independent influence on evapotranspiration. Overall, the ET at boreal forest sites shows a stronger dependence on relative humidity, and ET at tundra sites shows the stronger dependence on air temperature. These differences imply that tundra sites are more temperature-limited and boreal sites are more humidity-dependent. Relative to nearby unburned sites, the recovery time of ET after disturbance by wildfire was found to vary from several years on the Alaska tundra to nearly a decade in the Alaska boreal forest.

Table of Contents

List of Figures

List of Tables

1. Introduction

As the Arctic system evolves, a key question concerning its trajectory is: Will Arctic landscapes become wetter or drier as climate changes? A fundamental uncertainty surrounds the surface moisture budget and the relationship between precipitation (P) and evapotranspiration (ET). If P (including both rain and snow) exceeds ET over a period of time, the excess goes into runoff or storage. If ET exceeds P, the surface moisture deficit leads to drying unless there is sufficient recharge from below. A drying surface leads to decreased water supplies, increased wildfire risk, and moisture stress on vegetation, all of which have consequences for terrestrial ecosystems and human activities. These effects are most heavily felt by indigenous communities in the Arctic. Krupnik and Jolly, 2002 summarize several interview-based studies documenting the main changes indigenous communities have observed. Poor vegetation growth in some areas has been affecting the caribou and subsistence hunting has become more difficult with thinner caribou and poor-quality pelts. Warmer and drier conditions lower the soil moisture and water levels in surface lakes and rivers making travel from villages difficult in the warm season.

Global climate models have consistently projected increases of Arctic mean annual precipitation (IPCC, 2013, Figs. 11.12 and 12.22; USGCRP, 2017, Fig. 7.5), implying a wetter land surface in the future. However, there is a seasonality component to increased precipitation, with most of these increases occurring in the late autumn and winter (Bintanja and Selten, 2014). As summers become longer and warmer, increases of ET can be expected to offset at least some of the additional precipitation (Bring et al., 2016), and the IPCC even projects a future decrease of soil moisture in parts of the Arctic (IPCC, 2013, Fig. 12.23). By contrast, model-based studies project future increases of river discharge in the Arctic (IPCC, 2013, Fig. 12.24; Bring et al., 2016). The coarse resolution of these models and their rudimentary treatment of permafrost and

vegetative processes make it questionable to base conclusions about Arctic surface wetness trends on results from these simulations. Moreover, the trajectory of Arctic surface wetness is confounded by observations of decreasing soil moisture in the Arctic (Hinzman et al., 2013) and in subarctic Swedish basins where precipitation has been increasing (Destouni and Varrot, 2014). Earth system model results also show a reduction in wetland extent in higher latitudes, largely associated with permafrost thaw (Avis et al., 2011).

In a recent synthesis of Arctic terrestrial hydrology, Bring et al. (2016) conclude that "We are still lacking a comprehensive picture of evapotranspiration across Arctic regions and how it will interact with climate and landscape changes". Arctic hydrology is constrained by permafrost in its northern subregions, and changes in permafrost as well as vegetation will undoubtedly affect the trajectory of Arctic terrestrial hydrology, particularly the wetness of the surface. This thesis focuses on evapotranspiration (ET), especially its changes and variations relative to precipitation, one of the key drivers of terrestrial hydrology. A second topic of investigation in this study is the sensitivity of ET to various drivers, which include air temperature, humidity, wind, solar and longwave radiation, as well as the relationship between the surface fluxes of latent heat (ET) and sensible heat. The ability of models to capture these relationships will determine the validity of their simulations of the surface moisture budget and its changes.

Alaska serves as an attractive testbed for studies of variations in the surface moisture budget. It contains a range of biomes, including extensive areas of arctic tundra and boreal forest. It includes large regions underlain by permafrost, both continuous and discontinuous, as well as permafrost-free regions in its south. Finally, a network of research sites with eddy covariance flux towers has provided measurements of the surface fluxes of latent and sensible

heat in addition to the various other variables that represent drivers of the surface moisture budget. (The latent heat flux can easily be converted to ET by using the proportionality factor, the latent heat of vaporization). The flux tower sites in Alaska include the Japanese-operated supersite at Poker Flat as well as at two Long Term Ecological Research (LTER) sites, Bonanza Creek in the boreal forest and Imnavait Creek on the Arctic tundra. The present paper synthesizes measurements from flux towers in Alaska, together with measurements from other sites in northern high latitudes. The flux tower data include record lengths ranging from several months to more than a decade; much of the data is archived in repositories such as FLUXNET and AmeriFlux.

The results presented here include depictions of the seasonal cycle and interannual variations of evapotranspiration, with a focus on sites in Alaska. A metric of direct relevance to surface wetting and drying is P-ET. From an atmospheric perspective, P-ET is the net surface moisture flux, and we refer to it as such in the following sections. We also include an evaluation of the relative importance of various drivers of ET, with an eye towards the use of the results in model validation and calibration. We examine differences in the results for sites in different vegetation types and for sites with and without underlying permafrost. In order to document the surface moisture budget over Arctic land surfaces and to set the stage for model evaluations, we address the following questions:

1. How do surface moisture fluxes vary seasonally in different biomes and different permafrost regimes?
2. How do interannual variations of the net moisture flux compare with seasonal variations?
3. What is the relative importance of various atmospheric drivers of ET variations in different vegetation communities and permafrost regimes?

Finally, the moisture budget of the high-latitude land surface is affected by disturbance (wildfire, thermokarst, wetland drainage, deglaciation, insect outbreaks). Wildfire is especially important because, in most years, it affects millions of acres of boreal forest and tundra biomes. In recognition of the importance of wildfire as a major agent of disturbance of the high-latitude land surface, we include several sites with recent fire histories to illustrate the effect of wildfire on the surface moisture budget. In evaluating the interannual variations of the surface moisture fluxes at these sites, we address a final question:

4. Is there a detectable influence of disturbance by wildfire on the surface moisture flux, particularly during the early succession phase? If so, can a timescale of the effect on the surface moisture flux be identified?

Section 1 introduces the existing literature, Section 2 describes the datasets, the quality-control, and other processing steps used to prepare the eddy covariance data for analysis. Section 2 also describes two structural equation models used to quantify the relationships of ET to the various drivers. Section 3 contains the results on the seasonality and interannual variations of the surface moisture budget in different vegetation/permafrost regimes, the relative importance of various drivers of ET. Section 4 is a discussion of the results, while Section 5 contains a summary of the main conclusions.

2. Data and Analysis Methods

2.1 Data Processing

The focus of this analysis is on comparing the behavior of ET in tundra and boreal forest biomes with a focus on vegetation and permafrost differences. Station data from eddy covariance flux towers comprised most of the data used in this analysis. The flux towers at these

sites stand a few meters to tens of meters high and are mounted with instrumentation at various heights according to the measurement parameter and vegetation height. While eddy covariance measurements provided the estimates of the latent and sensible heat flux fluxes, precipitation and the other atmospheric variables are measured directly. The full list of variables used in this analysis is shown in Table 1 below.

Table 1. Variables measured at the flux tower sites.

Variable	**Variable Abbreviation**	**Units**
Latent heat flux	ET	W/m^2
Sensible heat flux	SHF	W/m^2
Incoming shortwave radiation	SW in	W/m^2
Outgoing shortwave radiation	SW out	W/m^2
Incoming longwave radiation	LW in	W/m^2
Outgoing longwave radiation	LW out	W/m^2
Air temperature	Ta	^oC
Precipitation	P	mm
Relative humidity	RH	%
Wind speed	WS	m/s
Ground heat flux	GHF	W/m^2

Datasets were accessed from AmeriFlux (https://ameriflux.lbl.gov), FLUXNET (https://daac.ornl.gov/cgi-bin/dataset_lister.pl?p=9), and/or through direct correspondence with the site's Principal Investigator (PI), A. Rocha. Sites were picked for this analysis to cover the tundra, forest, and permafrost categories with at least 3 years of data at each tower. The locations and key characteristics of the sites are listed in Table 2. For sites where the permafrost

status was unknown, estimations were made using the International Permafrost Association Arctic permafrost map (https://ipa.arcticportal.org/products/gtn-p/ipa-permafrost-map). Isolated and sporadic permafrost categories were considered non-permafrost for this analysis.

These data were processed into an aggregate standard half-hourly dataset for each station. Quality-control and, in some cases, gap-filling were performed by each site's PI. Data accessed from FLUXNET were gap-filled and processed according to the methodology described by Pastorello et al. (2020). Except for precipitation and latent heat flux, all variables listed in Table 1 were sorted as averages over daily, weekly and monthly periods for the analysis. For consistency with precipitation, the latent heat flux was converted to equivalent cumulative ET (mm/day) by using the latent heat of vaporization, thereby allowing direct comparisons and the calculation of differences such as P – ET. Net SW and LW radiation were calculated as incoming - outgoing such that a clear day would have positive net SW and a clear night would have negative net LW. Separate quality-controlled daily datasets were assembled with measurements adjusted for missing data by dividing by the fraction of data present.

Table 2. Eddy covariance measurement sites used in this study. Site id refers to the identifier associated with the Ameriflux or FLUXNET dataset when the data came from these databases.

Site ID	Site Name	Country	Latitude (°N)	Longitude (°N)	Vegetation	Permafrost	Data Coverage
CA-Man	Manitoba - Northern old black spruce	Canada	55.88	-98.48	Evergreen needleleaf forest	No	1994-2008
CA-NS1	UCI 1850 burn site	Canada	55.88	-98.48	Evergreen needleleaf forest	No	2001-2005
CA-NS2	UCI 1930 burn site	Canada	55.90	-98.52	Evergreen needleleaf forest	No	2001-2005
CA-NS3	UCI 1964 burn site	Canada	55.91	-98.38	Evergreen needleleaf forest	No	2001-2005
CA-NS4	UCI 1964 burn site wet	Canada	55.91	-98.38	Evergreen needleleaf forest	No	2001-2005
CA-NS5	UCI 1981 burn site	Canada	55.86	-98.49	Evergreen needleleaf forest	No	2001-2005
CA-NS6	UCI 1989 burn site	Canada	55.92	-98.96	Open shrublands	No	2001-2005
CA-NS7	UCI 1998 burn site	Canada	56.64	-99.95	Open shrublands	No	2001-2005
CA-SCB	Scotty Creek Bog	Canada	61.31	-121.30	Permanent wetlands	Discontinuous	2014-2017
CA-SCC	Scotty Creek Landscape	Canada	61.31	-121.30	Evergreen needleleaf forest	Discontinuous	2013-2016
DK-NuF /GL-NuF	Nuuk Fen (University of Copenhagen)	Greenland	64.13	-51.39	Permanent wetlands	Discontinuous	2008-2014

Table 2, continued.

DK-ZaF/GL-ZaF	Zackenberg Fen	Greenland	74.48	-20.55	Permanent wetlands	Continuous	2008-2011
DK-ZaH/GL-ZaH	Zackenberg Heath	Greenland	74.47	-20.55	Grasslands	Continuous	2000-2014
FI-Hyy	Hyytiala (U Helsinki)	Finland	61.85	24.29	Evergreen needleleaf forest	No	1996-2015
FI-Var	Varrio (U Helsinki)	Finland	67.76	29.61	Evergreen needleleaf forest	No	2016-2018
IS-Gun	Gunnarsholt	Iceland	63.83	-20.22	Deciduous broadleaf forest	No	1996-1998
RU-Cok	Chokurdakh (Vrije University Amsterdam)	Russia	70.83	147.49	Open shrublands	Continuous	2003-2014
RU-Fy2	Fyodorovskoye 2 (A.N. Severtsov Institute of Ecology and Evolution RAS)	Russia	56.45	32.90	Evergreen needleleaf forest	No	2015-2018
RU-Fyo	Fyodorovskoye (A.N. Severtsov Institute of Ecology and Evolution RAS)	Russia	56.46	32.92	Evergreen needleleaf forest	No	1998-2014
RU-Sam	Samoylov (University of Hamburg)	Russia	72.37	126.50	Grasslands	Continuous	2002-2014
RU-SkP	Yakutsk Spasskaya Pad larch (IBPC)	Russia	62.26	129.17	Deciduous needleleaf forest	Continuous	2012-2014
RU-Zot	Zotino	Russia	60.80	89.35	Permanent wetlands	No	2002-2004
SE-Fla	Flakaliden (Lund University)	Sweden	64.11	19.46	Evergreen needleleaf forest	No	1997-2002

Table 2, continued.

SE-Sk1	Skyttorp (SUAS Uppsala)	Sweden	60.13	17.92	Evergreen needleleaf forest	No	2004-2008
SE-St1	Stordalen Grassland (University of Copenhagen)	Sweden	68.35	19.05	Permanent wetlands	Discontinuous	2012-2014
SJ-Adv	Adventdalen (NATEKO)	Svalbard	78.19	15.92	Permanent wetlands	Continuous	2011-2014
US-A10	Utqiagvik (Barrow)	Alaska, USA	71.32	-156.61	Barren sparse vegetation	Continuous	2011-2018
US-An1	Anaktuvuk Severe Burn	Alaska, USA	68.98	-150.28	Open shrublands	Continuous	2008-2010
US-An2	Anaktuvuk Moderate Burn	Alaska, USA	68.95	-150.21	Open shrublands	Continuous	2008-2010
US-An3	Anaktuvuk Unburned	Alaska, USA	68.93	-150.27	Open shrublands	Continuous	2008-2010
US-Atq	Atqasuk	Alaska, USA	70.47	-157.41	Permanent wetlands	Continuous	1999-2006
US-Bn1	Bonanza Creek Delta 1920 Burn	Alaska, USA	63.92	-145.38	Evergreen needleleaf forest	Discontinuous	2002-2004
US-Bn2	Bonanza Creek Delta 1987 Burn	Alaska, USA	64.92	-145.38	Deciduous broadleaf forest	Discontinuous	2002-2004
US-Bn3	Bonanza Creek Delta 1999 Burn	Alaska, USA	63.92	-145.74	Open shrublands	Discontinuous	2002-2004
US-BZB	Bonanza Creek Thermokarst	Alaska, USA	64.70	-148.32	Permanent wetlands	Discontinuous	2013-2019
US-BZF	Bonanza Creek Fen	Alaska, USA	64.70	-148.31	Permanent wetlands	No	2013-2019
US-BZS	Bonanza Creek Black Spruce	Alaska, USA	64.70	-148.32	Evergreen needleleaf forest	Continuous	2010-2019
US-ICh	Imnavait Ridge	Alaska, USA	68.61	-149.30	Open shrublands	Continuous	2008-2018
US-ICs	Imnavait Fen	Alaska, USA	68.61	-149.31	Permanent wetlands	Continuous	2008-2018

Table 2, continued.

US-ICt	Imnavait Tussock	Alaska, USA	68.61	-149.30	Open shrublands	Continuous	2008-2018
US-Prr	Poker Flat Research Range Black Spruce Forest	Alaska, USA	65.12	-147.49	Evergreen needleleaf forest	Discontinuous	2010-2016
US-Rpf	Poker Flat Research Range deciduous forest	Alaska, USA	65.12	-147.43	Deciduous broadleaf forest	Discontinuous	2008-2019
US-Uaf	University of Alaska, Fairbanks	Alaska, USA	64.87	-147.83	Evergreen needleleaf forest	Discontinuous	2003-2017
YPF	Yakustk Pine (IBPC)	Russia	62.24	129.65	Evergreen needleleaf forest	Continuous	2004-2008
	Cherski (ETH Zurich)	Russia	68.64	161.33	Permanent wetlands	Continuous	2002-2005

Data coverage varied between sites with many missing winter data so the analysis was constrained to the warm season May through September. In some cases, variables were missing completely. Precipitation data from the ERA5 land hourly reanalysis (available at https://cds.climate.copernicus.eu/cdsapp#!/dataset/reanalysis-era5-land?tab=overview) was used to fill in missing precipitation data. To create the most complete dataset, timestamps where more than half the variables were missing were dropped. For the analysis methods discussed in sections 2.2 and 2.3, time series for each variable required at least 75% data coverage to be included.

2.2 Structural Equation Modeling Overview

With the large number of variables that have an influence on ET, a method was needed to identify those with the strongest relation to ET. Structural equation models (SEM) are commonly used to identify important variables among a large dataset. Multiple types of models fall under the broader category of SEM with the main differences being the types of variables being modeled and the relationships of those variables to the predictor variables in the dataset. Two SEMs were selected to be used in this analysis: a factor analysis and a path analysis. The factor analysis relates the variability within each variable in a dataset to a latent, unobserved variable and can show how variables behave similarly. This SEM does not remove underlying relationships between variables, allowing it to be influenced by the seasonal cycle within the dataset. A path analysis uses the observed variables within the dataset to predict another observed variable. This SEM allows effects from each variable to be independent from contributions from other variables. Together these SEMs allow conclusions to be made about the unique (independent) contributions of variables which are inter-related with other variables in the analysis.

2.3 Factor Analysis

The first SEM used in this analysis is a factor analysis which answers the question: how much common variance is shared among variables. UCLA: Statistical Consulting Group (https://stats.idre.ucla.edu/r/seminars/rcfa/#s2) provides an in-depth explanation of this model. There are two types of a factor analysis, exploratory and confirmatory. The UCLA: Statistical Consulting Group discusses a confirmatory factor analysis which attempts to predict a specified variable using the other variables in the dataset. An exploratory factor analysis was used in this

study to create an understanding of the behavior of groups of variables. However, the basic assumption of factor analysis is still the same for both methods "for a collection of observed variables there are a set of underlying factors that can explain the interrelationships among those variables" (UCLA: Statistical Consulting Group). The variability in a dataset as a whole is represented by a set of factors, each of which explains a certain amount of total variance in space and time. In each factor, each variable is given a loading (or weight) based on its contribution to the variance explained by that factor. The first factor is essentially the linear combination of the variables that explains the maximum amount of variance in the overall dataset. The second factor explains the maximum of the variance that is unexplained by the first factor; and so on, with each successive factor maximizing the variance unexplained by the preceding factors but explaining successively smaller fractions of the overall variance. Multiple variables can have strong loadings in the same factor, indicating they follow a similar pattern and are likely highly related. Therefore, inclusion of a target variable (ET, in this case) can show which variables have the strongest association with the target variable. The Python3 factor-analyzer package was used to run the model. The factor analysis was run separately for the daily, weekly, and monthly aggregate values.

2.4 Path Analysis

To understand how each variable contributes unique information to variability in ET, a path analysis was used. This SEM is commonly used in comparing direct effects of meteorological variables onto ET. Zhang et al. (2015) used a path analysis in a similar application to compare the effects of net radiation, air temperature, vapor pressure deficit, and wind speed on ET. The UCLA: Statistical Consulting Group also describes the path analysis and

similar models in depth (https://stats.idre.ucla.edu/r/seminars/rsem/). A path analysis is a specific type of SEM which uses a set of exogenous variables (variance is independent of other variables) to predict endogenous variables (variance is dependent on other variables) while allowing the variables to predict each other in the process. This analysis used the R lavaan package SEM function to define and run the model to predict ET using precipitation, temperature, relative humidity, windspeed, sensible heat flux, ground heat flux, net shortwave, and net longwave radiation. Specific covariances between exogenous variables were not defined for the model but are presented in Section 3.3 based on separate calculations. This model produces a matrix of regression estimates, standard error, z-value, and p-value for each variable. The regression coefficients produced by the model represent the slope of the linear relationship between each variable and the predicted variable independent of all other variables. The model was run on the daily and weekly timescales to have a sufficiently large sample size for model confidence.

To test the significance of differences in regression coefficients between variables, the Kruskal-Wallis test was run for three groups of variables. The Kruskal-Wallis test (Kruskal and Wallis, 1952) is a measure of the significance of differences between two or more distributions, however it does not specify which and how many of the included distributions are significantly different. The first test included all variables in the model. The second included windspeed, temperature, and ground heat flux, and the third test only included temperature and ground heat flux. Only regression coefficients with significant p-values ($p \leq 0.05$) were kept for the analysis. This path analysis allows direct relationships between ET and predictor variables to be measured. Variables with large regression coefficients can be interpreted to have a large influence on ET.

Combining the results from the factor analysis and path analysis, variables with similar behavior and those which influence ET independently can be identified.

3. Results

3.1 Seasonal and Interannual Variations

To illustrate the seasonality of the surface moisture budget components, we present the calendar-month means and corresponding ranges for the different vegetation types and permafrost status. A sample of data-rich sites were selected for the moisture budget analysis to include tundra (US-ICs, US-ICh, US-ICt, and US-A10) (including shrub tundra and wetland tundra sites) and boreal forest (including deciduous broadleaf and evergreen needleleaf). The boreal forest sites were then grouped into subsets with permafrost (US-Prr, US-Rpf, US-Uaf, RU-Skp, and US-BZB) and without permafrost (FI-Hyy, RU-Fyo, and US-BZF). As shown in Figure 1, the seasonal cycle of precipitation is qualitatively similar for all three categories of sites, with maximum amounts during the warm season (June through August). These months also have larger interannual ranges compared to the cold-season months, with July and August showing the largest range at the forest sites underlain by permafrost and August showing the largest range in the tundra sites. The monthly median values for the non-permafrost sites are generally higher than for either category of the permafrost sites. This difference in median values is consistent with the fact that precipitation generally increases southward. The non-permafrost sites tend to be located further south than the permafrost sites.

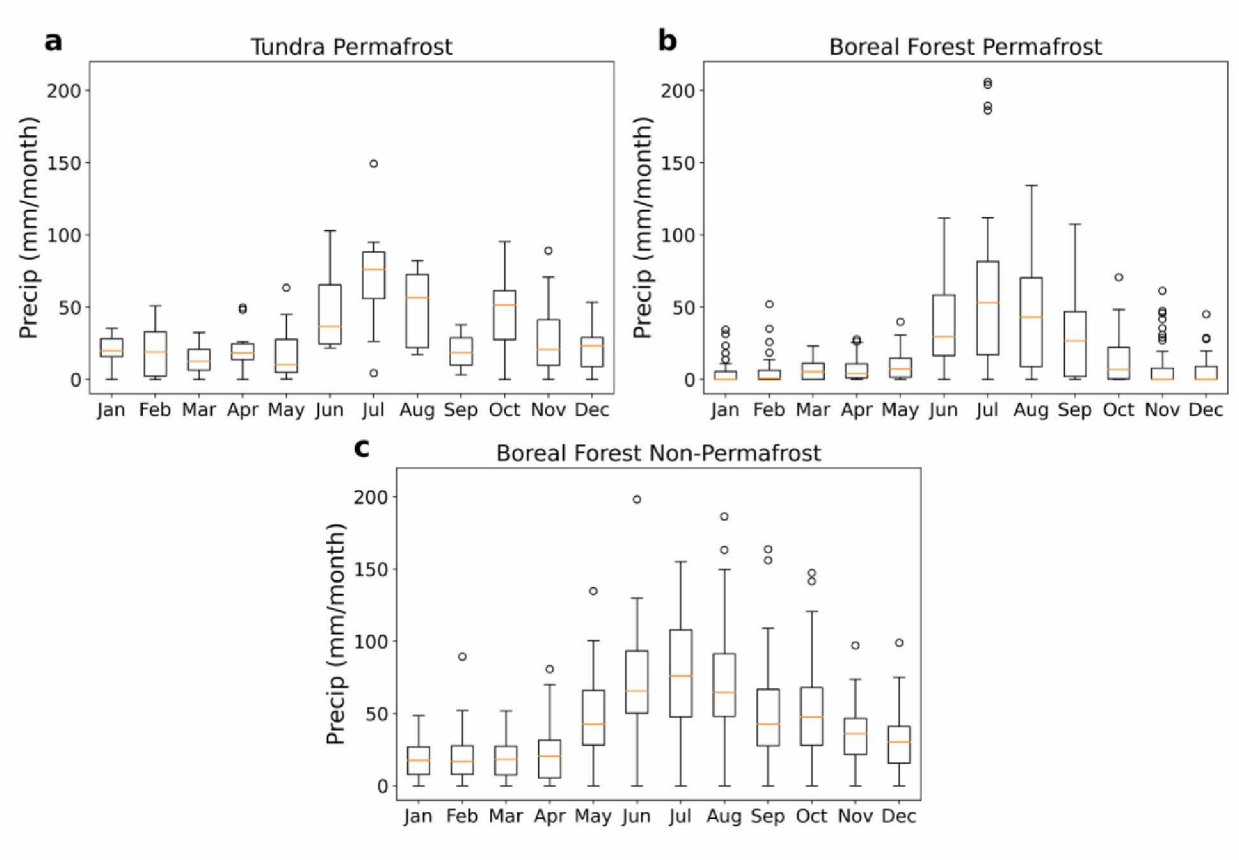

Figure 1. Composite distributions of total monthly precipitation (a) tundra, (b) boreal forest permafrost, and (c) boreal forest non-permafrost sites. Orange lines are median values, boxes represent interquartile range, and whiskers 1.5 times the interquartile ranges. Open circles are statistical outliers.

The seasonal cycles of ET are shown in Figure 2. ET for the boreal forest sites shows a similar seasonal cycle to precipitation, although the springtime increase occurs somewhat earlier, as the April and May values are larger relative to the July maximum in comparison with the seasonal cycle of P. ET also shows less interannual variability than does P (note the different scales in Figure 2). At tundra sites, ET starts increasing in May with a maximum in July. The annual sum of the median values of ET is approximately 140 mm for tundra sites, 224 mm for boreal forest permafrost sites, and 313 mm for non-permafrost boreal forest sites. The

interannual variability of ET is larger at tundra sites with a range from 0 mm to about 75 mm in July alone.

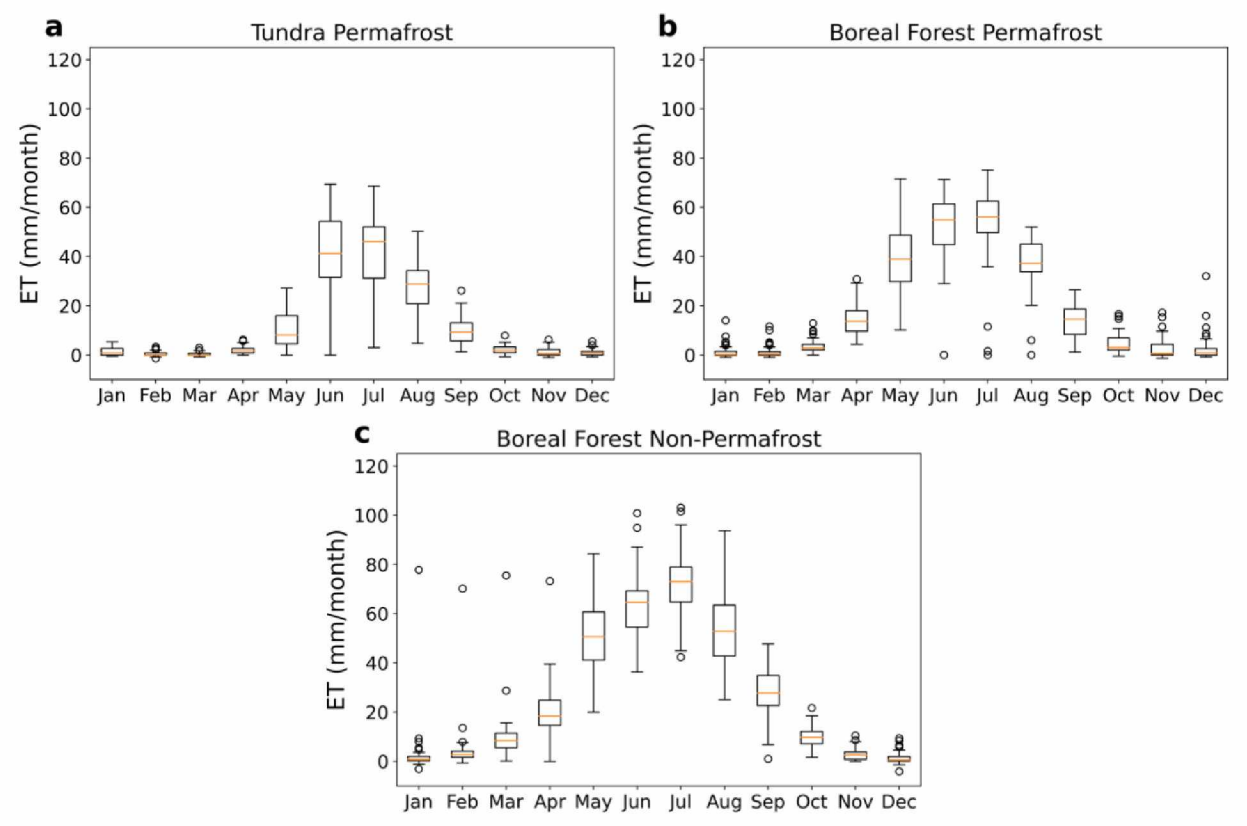

Figure 2. As in Figure 1, but for total monthly evapotranspiration (ET).

Finally, Figure 3 shows the net surface moisture flux, P-ET for the different vegetation types. The P-ET cycle for tundra sites shows predominantly positive medians. The interannual variability is largest in July. At the boreal forest sites with permafrost, the seasonal cycle of P-ET varies from negative in the spring to positive in the summer and autumn. However, the interannual variability is large, with both positive and negative values in June, July, August, and even September. Most years have a moisture deficit (negative P-ET) in May, when precipitation

is low, and a moisture surplus in September. By contrast, the non-permafrost boreal forest sites have median values close to zero in spring, although the interannual variability is large throughout May - October. Over the warm season, there is a slight positive shift in the median with all months still having both positive and negative values. The sum of the median values of P-ET is approximately +210 mm for tundra sites, -55 mm for boreal forest permafrost sites, and +175 mm for non-permafrost boreal forest sites, indicating a net flux of moisture from the atmosphere to the surface at the tundra and non-permafrost boreal forest sites. All three values are likely underestimates of the annual net P - ET because winter precipitation is not measured at many of the locations. For this reason, the negative value for the boreal forest permafrost sites may well be unrepresentative of the actual annual net moisture exchange with the atmosphere, as it implies a moisture loss that would need to be offset by net inflow at or below the surface.

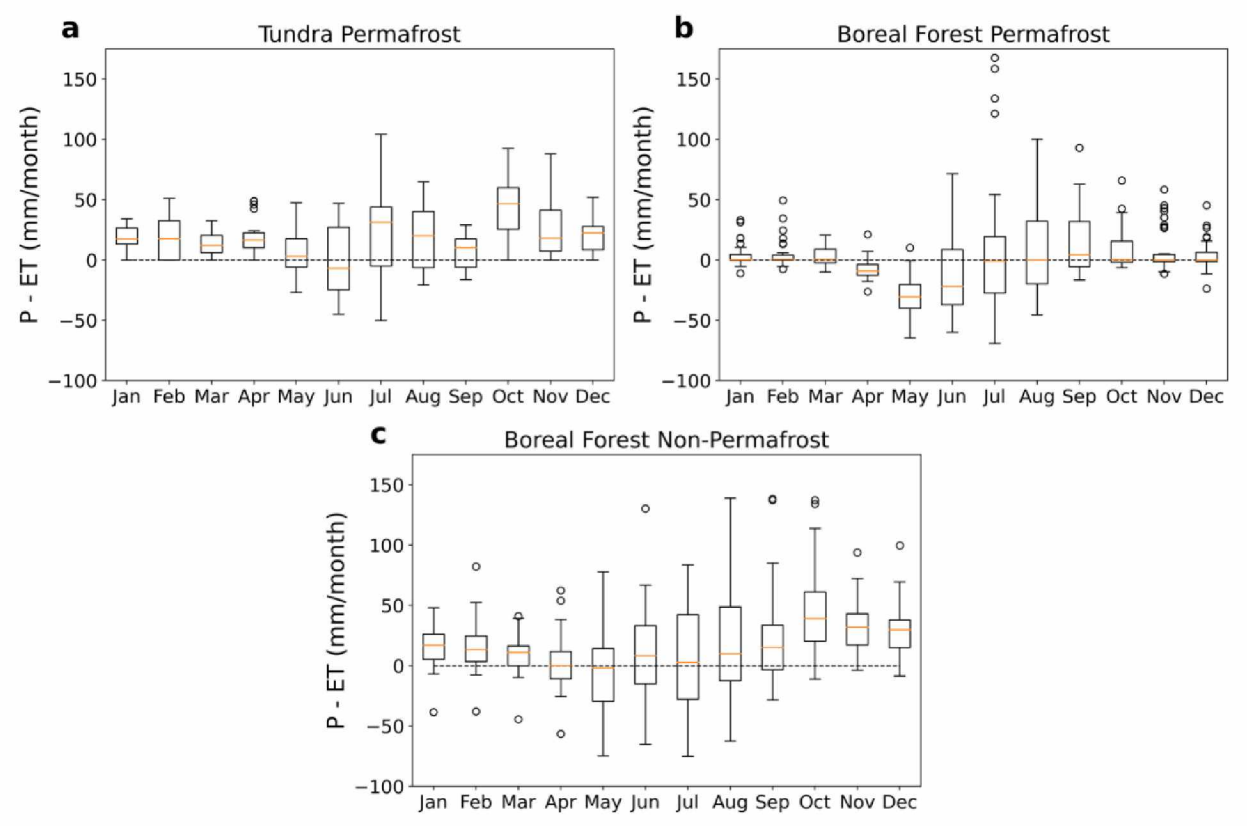

Figure 3. As in Figure 1, but for total monthly precipitation minus evapotranspiration (P – ET).

Differences between the P-ET regimes of the boreal forest sites with and without permafrost are apparent in Figures 3b and 3c. In addition to the absence of a moisture deficit in spring, the non-permafrost sites show generally greater ranges of interannual variations. The role of permafrost in these differences is discussed in Section 4.

Interannual variability of the net surface moisture fluxes is large and tends to be damped by the compositing used to construct Figures 1-3. For this reason, we use the fluxes at the Poker Flat black spruce site, to illustrate the interannual variability of the yearly net moisture gain or loss (Figure 4). The annual curves represent the accumulated P-ET beginning on January 1 and

continuing through the end of each year. It is apparent that there is a net loss of moisture by the surface (negative P-ET) in the early part of the growing season, typically beginning in mid-May when ET generally exceeds P. The recovery to a net positive value of the cumulative P-ET occurs later in the year, although the time of the recovery varies from late June (2014) to November (2013). The yearly total moisture gained by the surface ranges from about 15 mm in 2013 to nearly 300 mm in 2014, which was an exceptionally wet year in Interior Alaska.

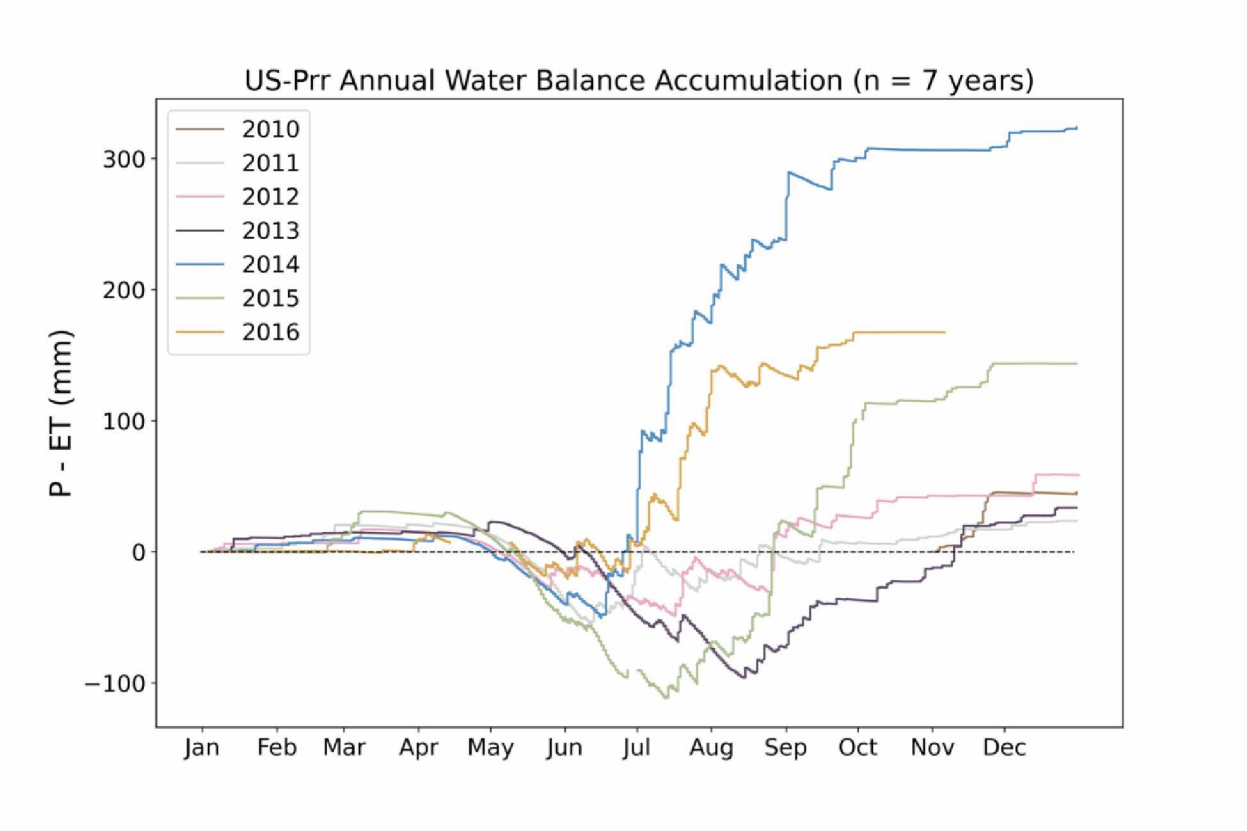

Figure 4. Yearly cumulative totals of P-ET at Poker Flat black spruce site, US-Prr. Years are color-coded according to legend in upper left corner.

As shown in the appendix, positive water balance years are most frequent at most sites. However, the Imnavait Creek sites as well as the Bonanza Creek fen show a roughly equal

spread between positive and negative annual water balance (Figure A4). The Bonanza Creek thermokarst (US-BZB), on the other hand, shows a mostly positive annual water balance with the exception of 2017. Positive annual water balances were also obtained for the US-Rpf, US-Prr, FI-Hyy, RU-Fyo, and US-BZB sites with only a few dry years resulting in a negative water balance. On the other hand, the US-Uaf site showed a negative water balance in most years. Due to data limitations at the RU-SkP site, specifically the absence of winter precipitation measurements, the sign of the water balance cannot be confidently concluded for this site.

3.2 Effects of disturbance

Several high-latitude flux towers in the AmeriFlux and FLUXNET databases are located in fire scars undergoing wildfire recovery. The Poker Flat Deciduous Burn (US-Rpf) site, which is one of the burn sites examined by Ueyama et al. (2019), experienced a boreal forest wildfire in 2004, while the Anaktuvuk River severe and moderate burn sites (US-An1, US-An2) examined by Rocha et al. (2011), are in the burn scar of the large wildfire in tussock tundra on the North Slope of Alaska that occurred in 2007. Here we examine the post-wildfire evolution of evapotranspiration at these sites. Figure 5 shows the June, July, and August values of ET at the Poker Flat sites (blue) and Anaktuvuk River sites (orange). Measurements at Poker Flat have been made at the site of the 2004 wildfire and at an adjacent site that did not burn. The sites at Anaktuvuk River are made over areas which experienced the 2007 wildfire to varying severities. The time-variations in the Poker Flat burned site show positive trends in both June and July. The June, July, and August trends account for 39%, 42%, and 3% of the variance, respectively, with the June and July trends statistically significant ($p < 0.05$). One may hypothesize that the increase in ET is related to variations in precipitation. However, additional analysis (Figure 6)

showed that the correlations with precipitation are not significant in any month. Moreover,

Figure 5 shows no significant trends at the unburned Poker Flat site.

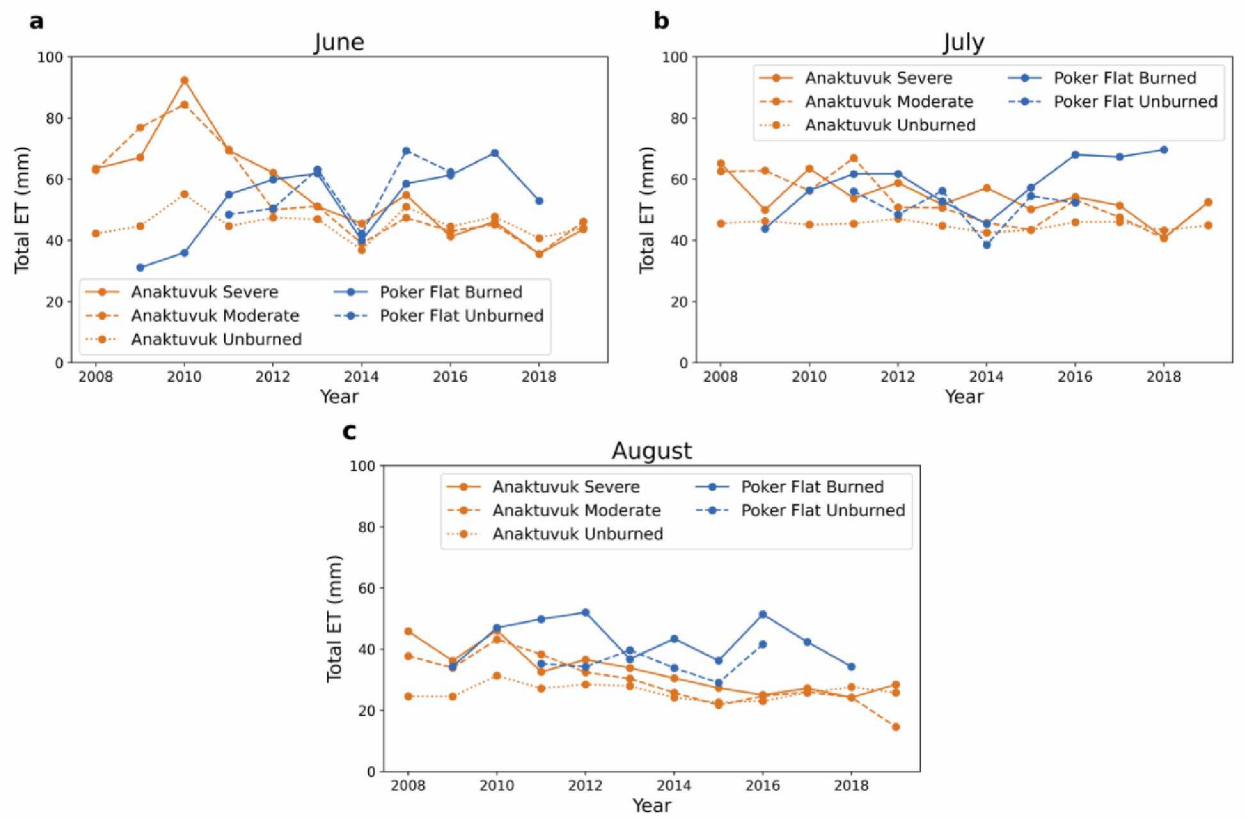

Figure 5. Time history of ET at the Poker Flat deciduous burn (US-Rpf), Poker Flat black spruce (US-Prr), Anaktuvuk River severe (US-An1), moderate (US-An2), and unburned (US-An3) sites during (a) June, (b) July and (c) August.

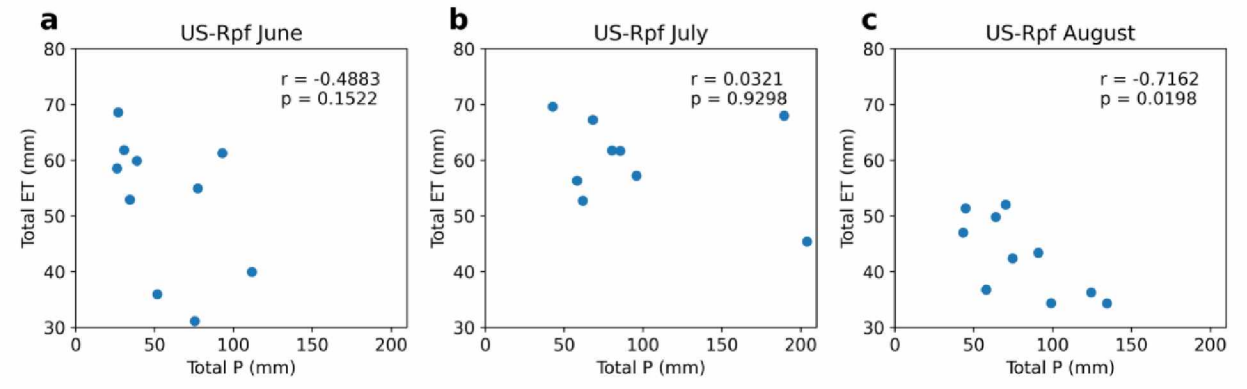

Figure 6. Scatter plots of monthly total ET vs. monthly total precipitation at the Poker Flat burn site for (a) June, (b) July and (c) August, with corresponding correlations (r) and significance levels (p) in upper right of each panel.

A similar comparison can be made for the 2007 Anaktuvuk tundra fire, for which the measurements span 2008-2019. Values of monthly ET at each of these sites are also shown in Figure 5 for June, July and August. May is not included in the figure because the tundra is generally completely snow-covered until the end of May or early June. The Anaktuvuk sites are distinguished by in Figure 5 severe burn (US-An1), moderate burn (US-An2) and unburned (US-An3). Both burned sites show an increase in ET during the first three years post-fire, followed by a decrease in ET over time after three years. For the entire period (2008-2019), the negative trends of ET are statistically significant ($p < 0.01$) at both the moderate and severe burn sites in June and August, and marginally significant ($p = 0.03$ and $p = 0.12$) for the moderate and severe burn sites in July. At the unburned sites, all three monthly trends are insignificant ($p > 0.30$).

3.3 Factor Analysis

As noted in the Introduction, various atmospheric variables may contribute to variations of ET: air temperature, precipitation, relative humidity, wind speed, shortwave and longwave radiation, as well as the partitioning of the available energy into sensible heat, the flux of heat into the ground, and evapotranspiration. Figure 7 shows the correlation matrix for all sites at the daily, weekly, and monthly scales between all variables as an initial investigation into these relationships. In these correlation plots, ET correlates highly ($|r| > 0.5$) with net shortwave radiation, ground heat flux, and temperature on the daily, weekly, and monthly scales with sensible heat flux becoming highly correlated at the monthly scale. Precipitation and windspeed have low ($|r| < 0.25$) correlation with ET on all timescales. Net shortwave radiation has the largest correlation with ET and is also highly correlated with relative humidity, sensible heat

flux, ground heat flux, and net longwave radiation on all timescales. Generally, these correlations increase in magnitude as the timescale increases.

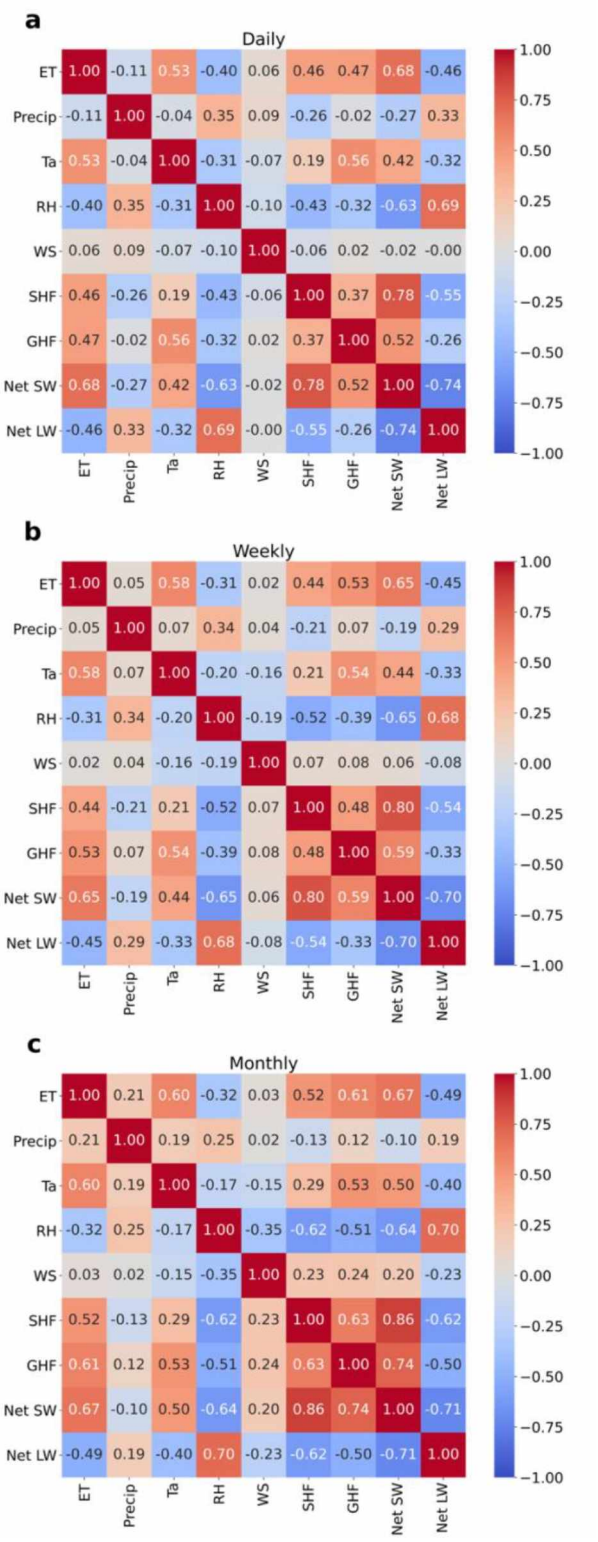

Figure 7. Correlation matrixes between all variables from all sites at the daily, weekly, and monthly scales.

As shown in the correlation plots above, many of these variables share similar behaviors and a method is needed to quantify the contribution of each variable to variability patterns. The factor analysis described in Section 2.2 was run across all sites and variables listed in Tables 1 and 2 to categorize these variables into groups showing similar variability. Figure 8 shows the first factor loadings for tundra, forest, and non-permafrost forest sites. ET, temperature, sensible heat flux, ground heat flux, net shortwave, net longwave, and negative relative humidity all load highly on the first factor. Windspeed and precipitation have low factor loadings, with the precipitation loadings becoming more positive with increased timescale. The main differences between forest, tundra, and permafrost is that relative humidity tends to load more strongly negative for forest sites than tundra. Temperature also loads lower for non-permafrost sites than the permafrost sites.

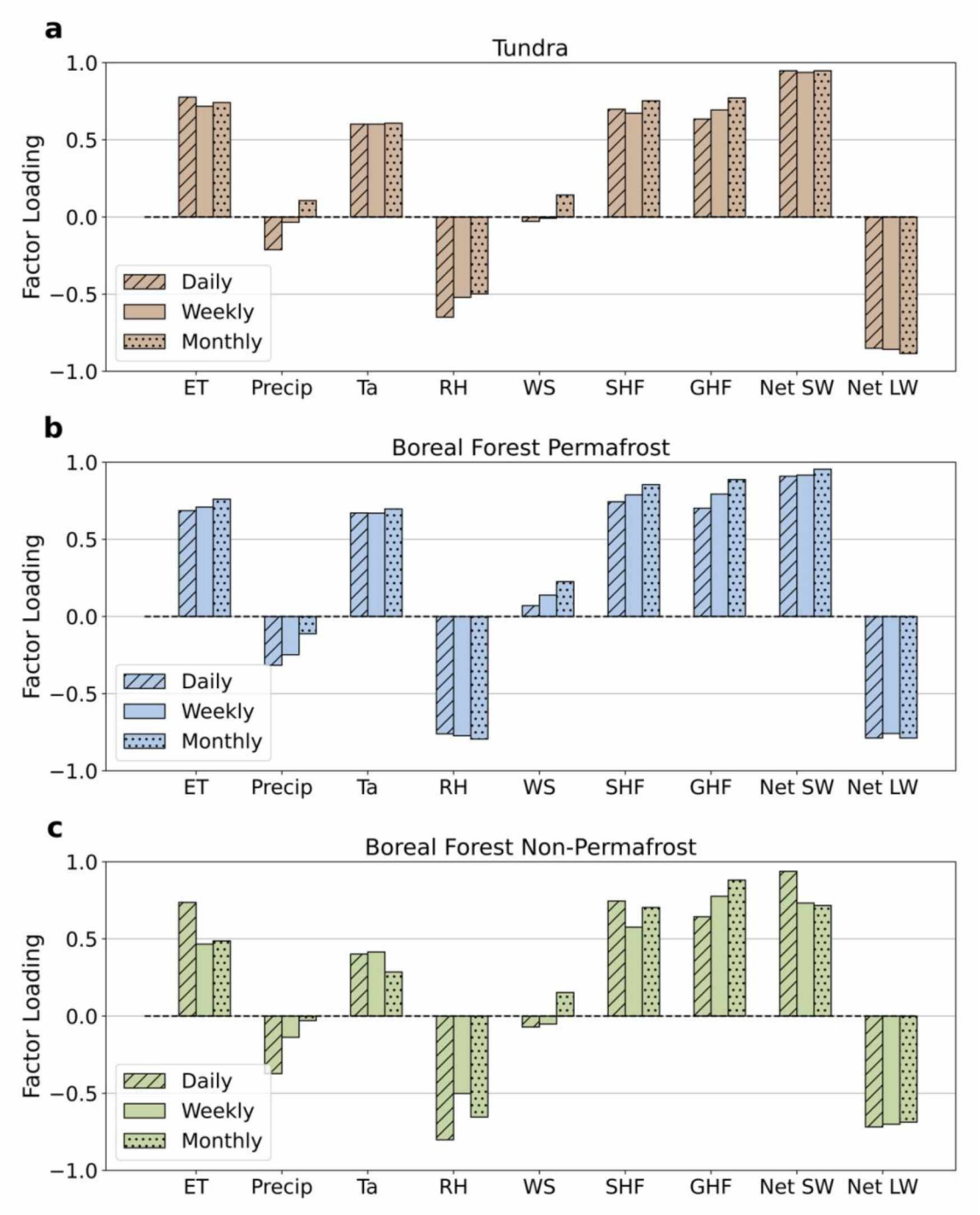

Figure 8. Loadings of variables in the first pattern of the factor analysis for (a) tundra (b) forest permafrost, and (c) forest non-permafrost sites.

The factor analysis produces multiple factor loadings with the first factor capturing approximately 50% of the variability in the dataset. Scoreplots were made to show the loadings on both the first and second factors for all variables. Figure 9 shows scoreplots grouped by tundra, forest, and non-permafrost forest sites similar to the groupings in Figure 8. All individual sites are shown by the muted markers, categorized by color and time scale (daily, weekly, and monthly), and the average factor loadings for each group are shown by the fully saturated and outlined markers. This figure shows the same results as Figure 8, however the spread among sites is apparent. Precipitation and windspeed have a large spread in both factors with the average second factor loading slightly positive for precipitation. Tundra sites show a more consistent spread in the first factor for the thermal variables ET, temperature, and sensible heat flux.

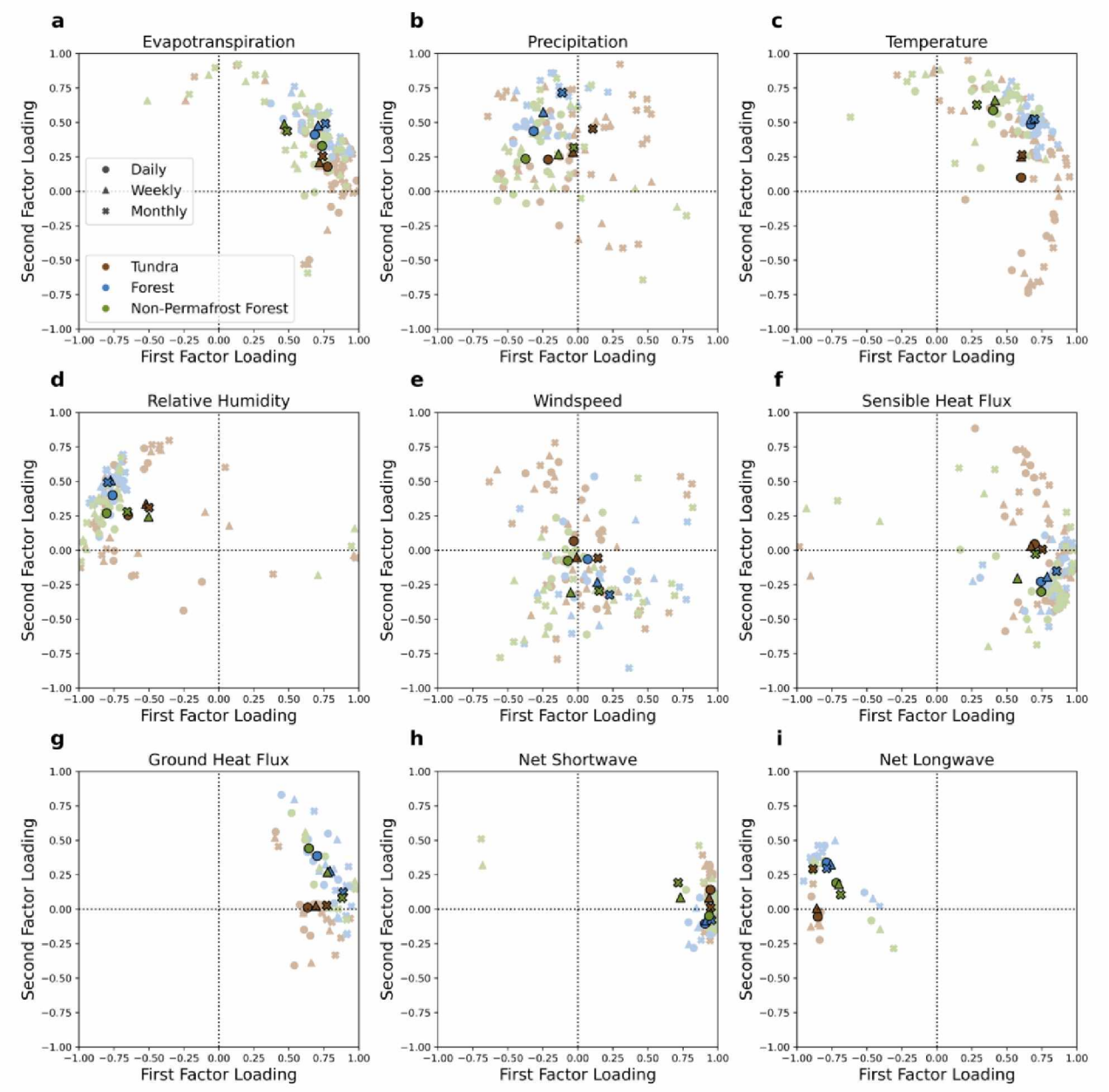

Figure 9. Scoreplots of the first and second factor loadings for each variable at the daily, weekly, and monthly timescales. Sites are categorized by tundra (brown), boreal forest with permafrost (blue), and boreal forest without permafrost (green). Muted datapoints show individual site loadings and fully saturated points show the average loadings for the corresponding category.

It is also useful to compare the factor loadings by permafrost presence or absence.

Figures 10 and 11 show scoreplots for tundra and forest, respectively, with sites grouped by

permafrost status. Consistent with Figure 9, ET, temperature, sensible heat flux, ground heat flux, net shortwave, net longwave, and negative relative humidity load highly on the first factor for all permafrost groups in both tundra and forest. The low factor loadings for temperature at the non-permafrost forest sites in Figure 8c are supported by a decreasing trend in factor loading as permafrost status decreases in Figures 10 and 11 for both tundra and forest. ET shows a similar relationship to temperature for the tundra sites, however this pattern is not apparent in the forest sites.

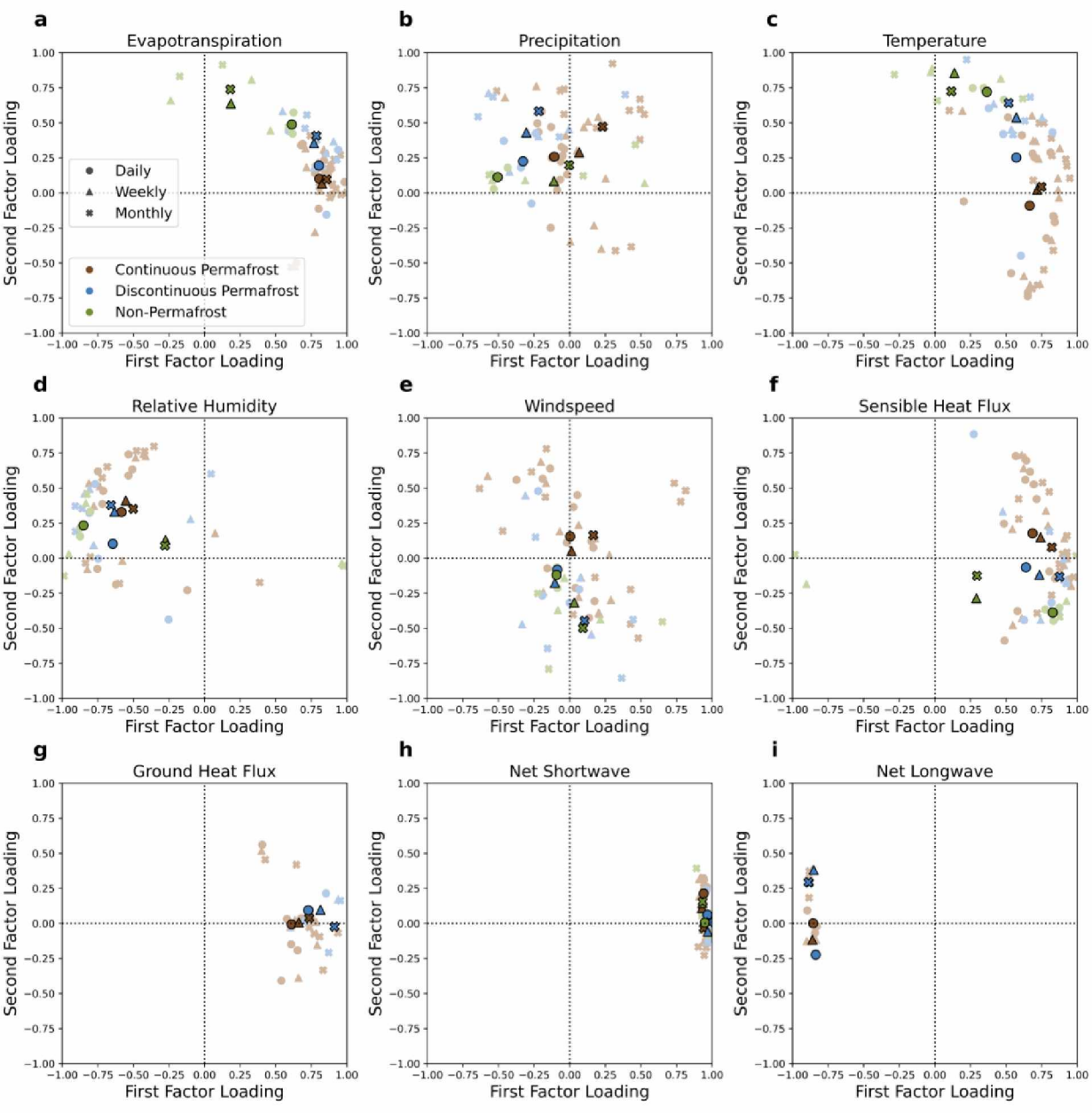

Figure 10. As in Figure 9, but for tundra sites with continuous permafrost (brown), discontinuous permafrost (blue), and non-permafrost (green).

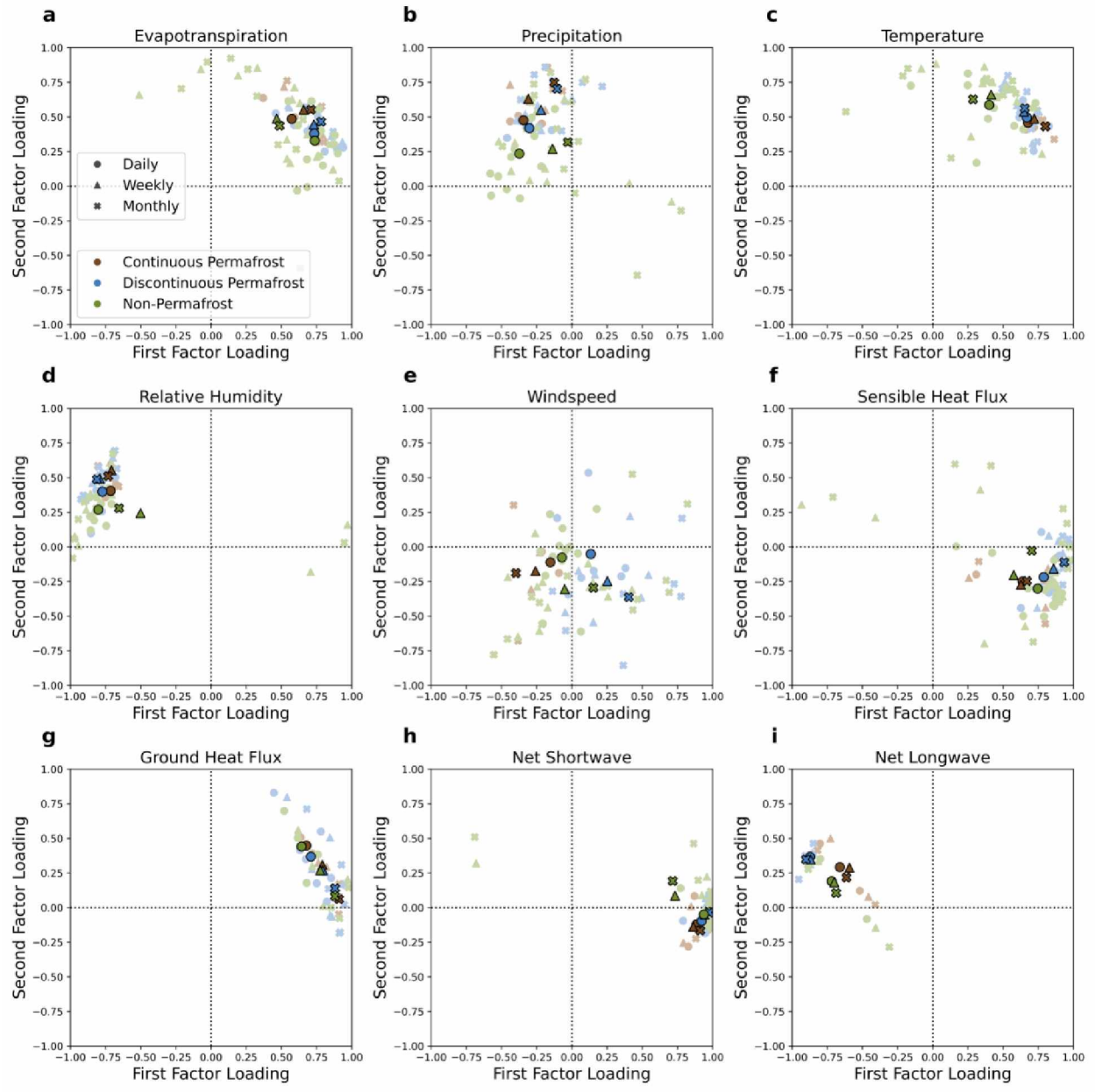

Figure 11. As in Figure 9, but for boreal forest sites with continuous permafrost (brown), discontinuous permafrost (blue), and non-permafrost (green).

The final comparison in this analysis was to group the factor loadings by vegetation type for forest and tundra sites. Figures 12 and 13 show scoreplots for tundra and forest sites grouped by vegetation type: shrubland, wetland, and grassland for tundra, and deciduous needleleaf,

wetland, evergreen needleleaf, and deciduous broadleaf for forest sites. Most tundra sites fall under the shrubland and wetland categories with 2 sites in the grassland category. The majority of the forest sites were evergreen needleleaf forest with 6 sites making up the remaining categories. For the tundra, the 2 grassland sites loaded distinctly lower on the first factor than shrubland and wetland sites for relative humidity. This indicates that for the grassland sites, relative humidity does not follow as similar a pattern to ET than the shrubland and wetland sites. Shrubland sites loaded slightly lower than other sites for ET, temperature, and sensible heat flux, and loaded distinctly more positive on windspeed. In general, the forest sites show a larger spread in the first factor for ET, temperature, and sensible heat flux and a lower spread in relative humidity than the tundra sites. Windspeed is slightly negative in the second factor loading and precipitation is slightly positive.

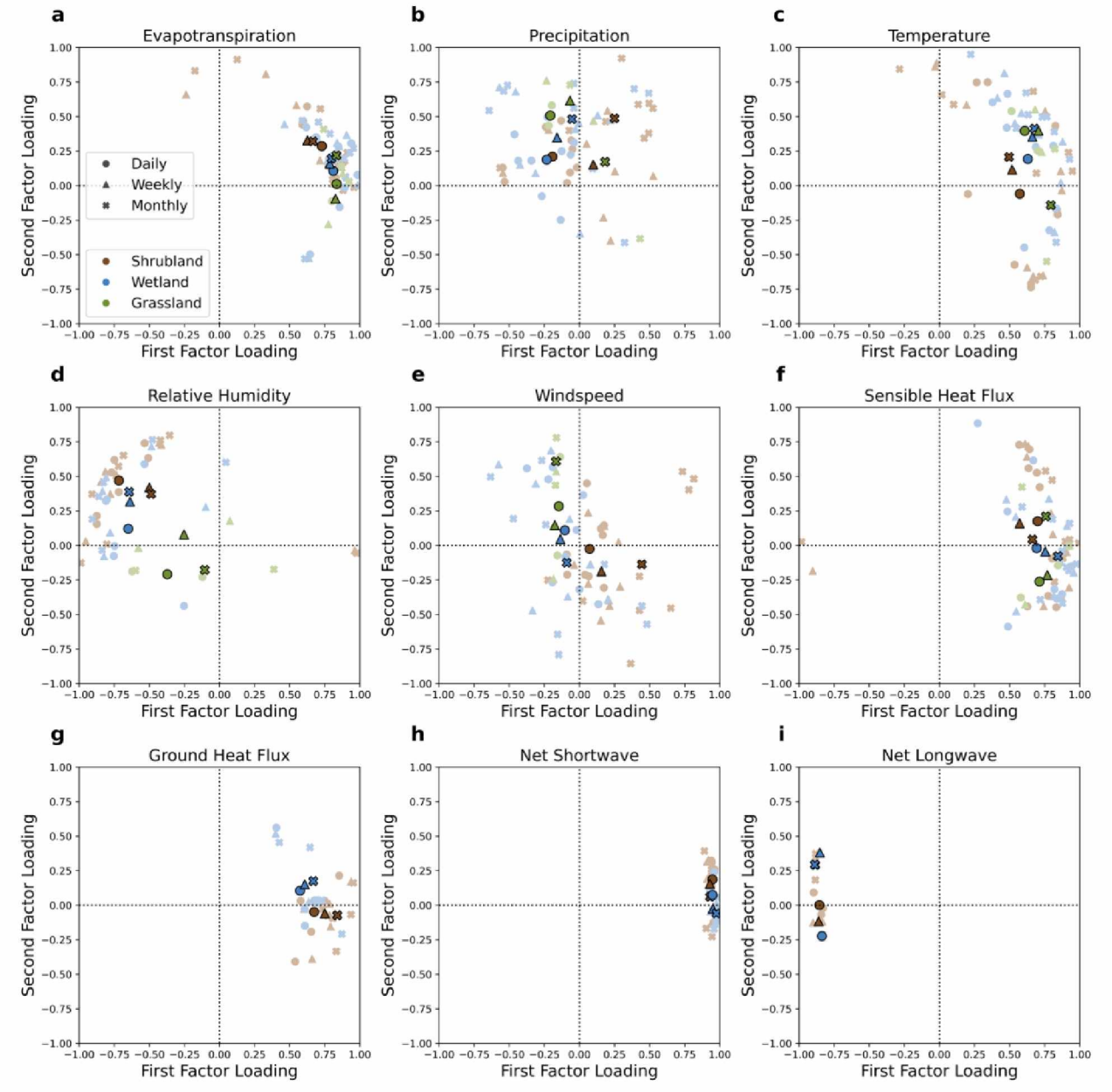

Figure 12. As in Figure 9, but for tundra sites in open shrubland (brown), wetland (blue), and grassland (green) vegetations.

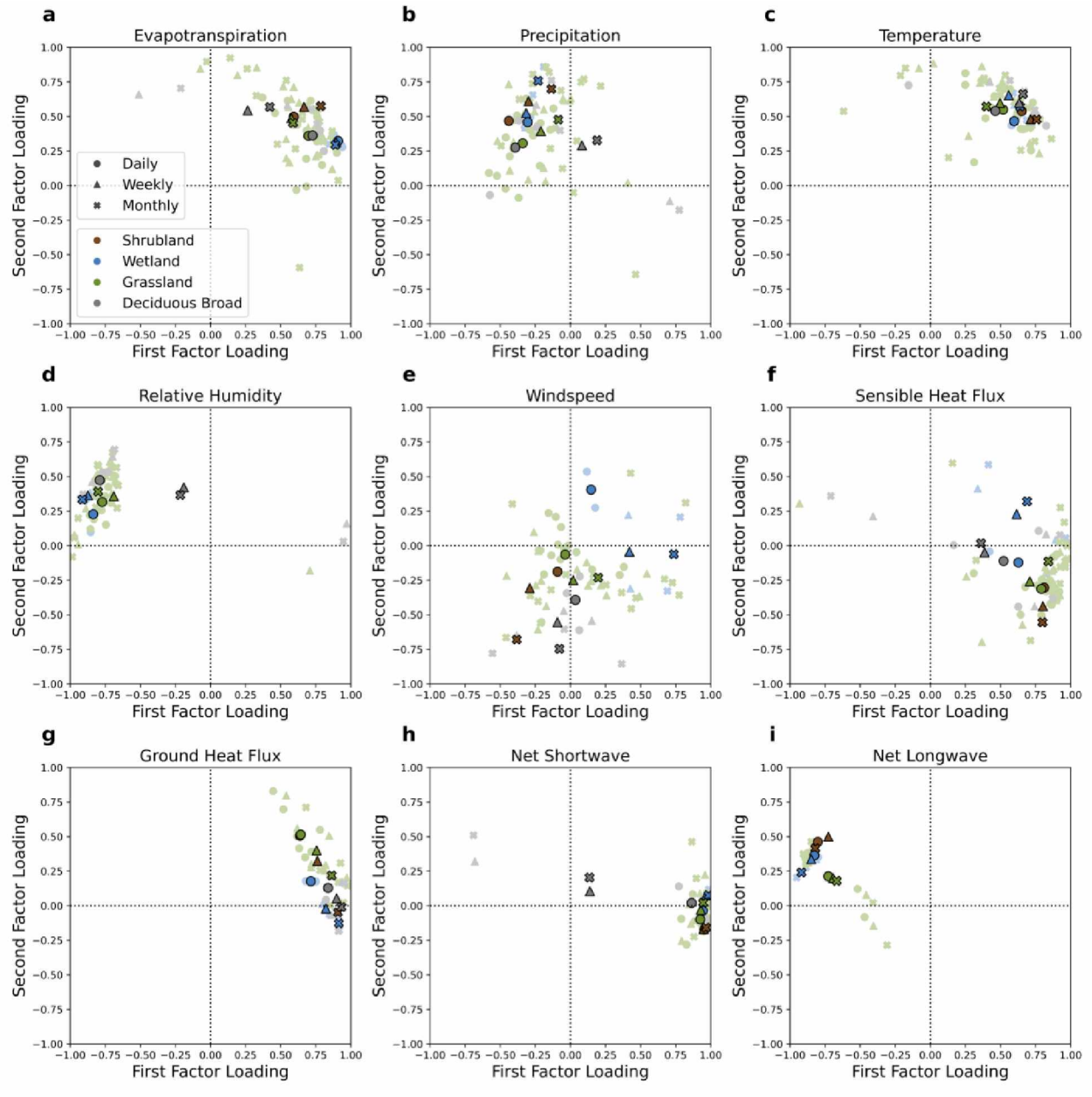

Figure 13. As in Figure 9, but for forest sites in deciduous needleleaf (brown), wetland (blue), evergreen needleleaf (green), and deciduous broadleaf (gray) vegetations.

3.4 Path Analysis

While a factor analysis quantifies relationships among a complex set of inter-correlated variables, correlations deduced from factor loadings do not provide measures of correlation with

a variable after removal of the effects of other inter-correlated variables. Therefore, we supplement the factor analysis with a path analysis to quantify the direct dependencies of ET on each variable independent of all other variables. Figure 14 shows the distribution of regression coefficients for each variable from all runs of the path analysis at the daily, weekly, and monthly scales. Windspeed stands out having both the largest regression coefficient and largest spread in coefficients. The scale of the regression coefficients increases with increased timescale, noting the different y-axis scales in Figure 14. This is a product of the large timescales being sums of the smaller timescale values. The results shown here include extreme outliers in both windspeed and ground heat flux. Results from the path analysis are subject to error from small sample size and poor model fit. When comparing results of the path analysis across vegetation and permafrost status, only those results with significant p-values were included. Figure 15 shows the combined results of the path analysis for only significant p-values at the 95% confidence interval; this restriction excludes results with both poor model fit and low sample size. Model runs at the monthly scale were mostly all insignificant with low sample size so only the daily and weekly runs were included for the analysis. Windspeed continues to stand out with the highest median regression coefficient for all sites, with temperature and ground heat flux as the next largest coefficients respectively.

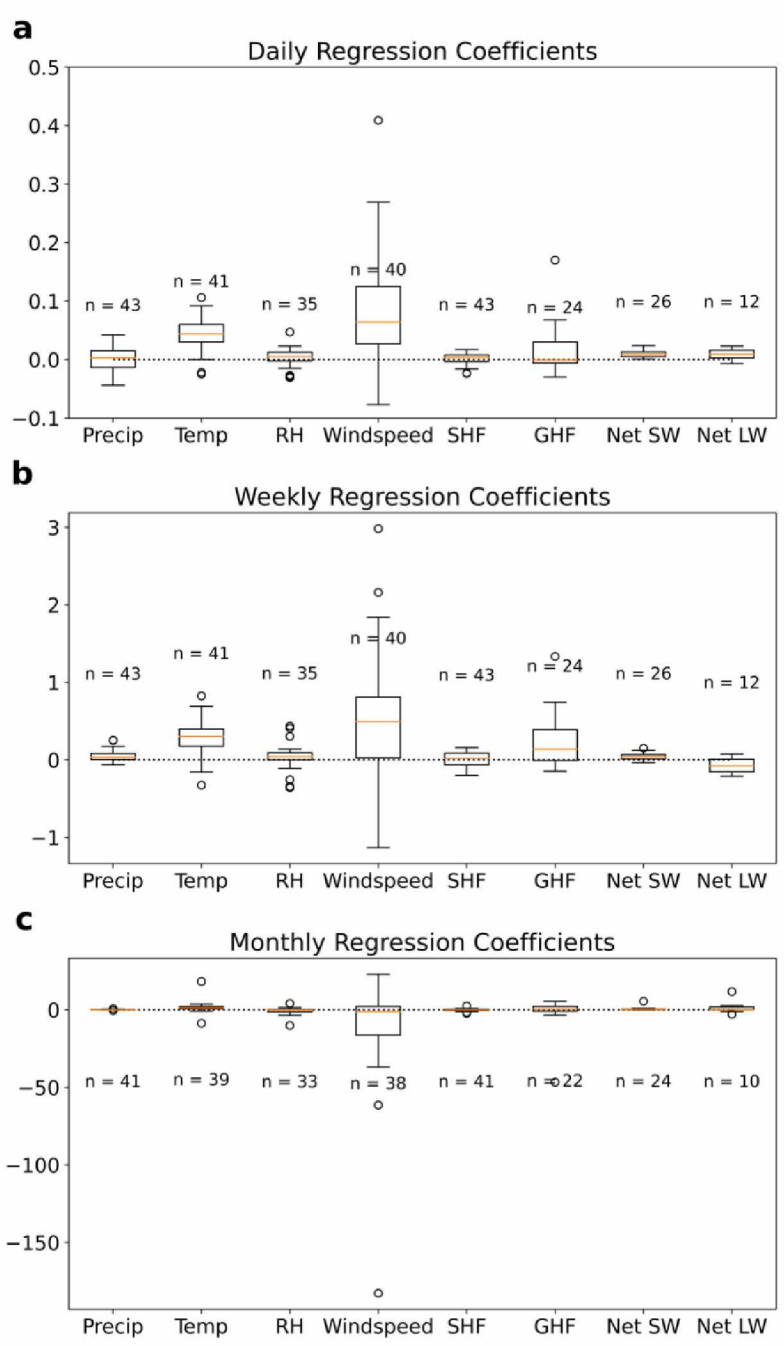

Figure 14. Distributions of regression coefficients from all results of the path analysis SEM at the daily, weekly, and monthly scales. Orange lines are median values, boxes represent interquartile range, and whiskers 1.5 times the interquartile ranges. Open circles are statistical outliers. Sample sizes are given for each variable.

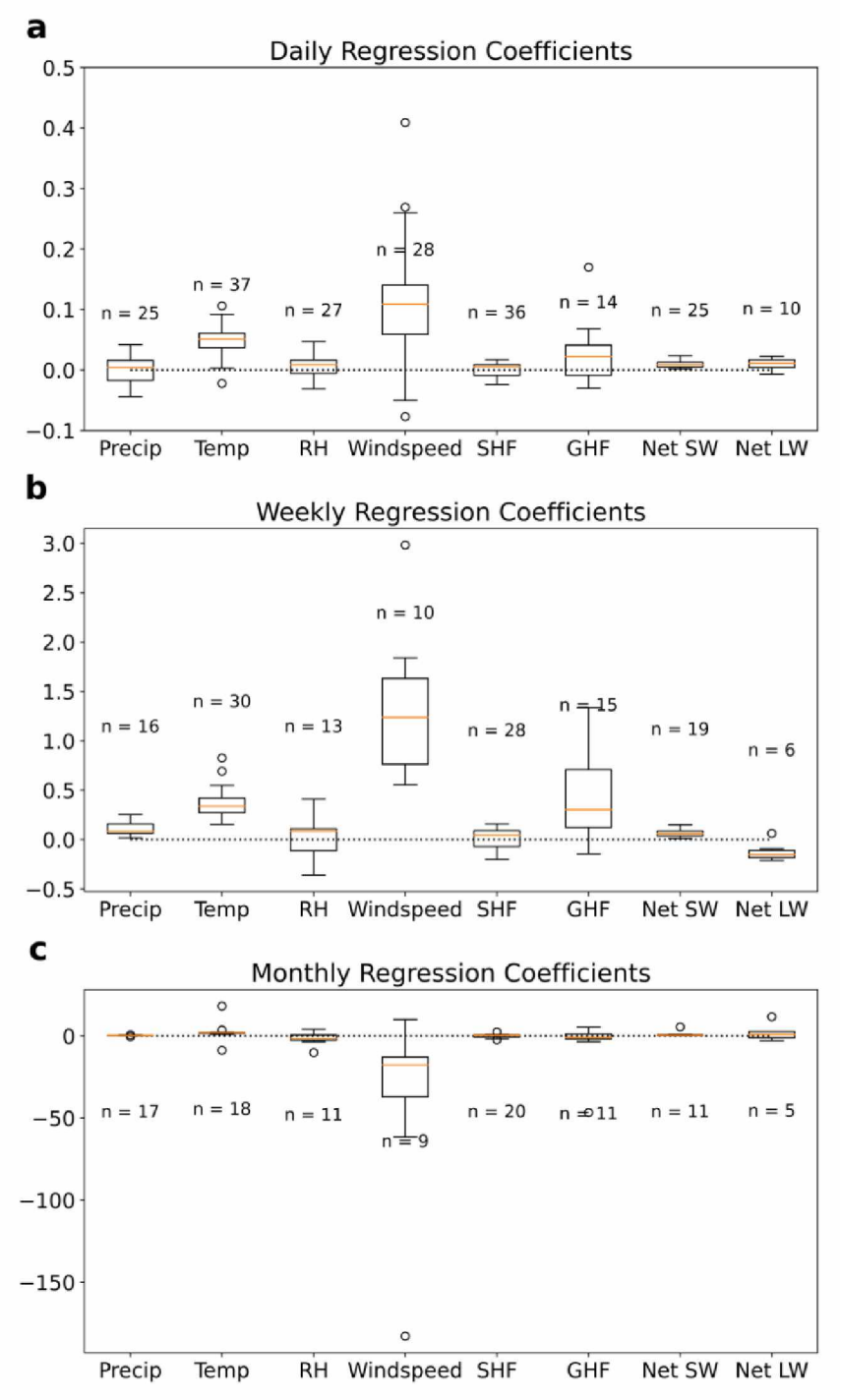

Figure 15. As in Figure 14, but for statistically significant regression coefficients at the 95% confidence interval.

Similar to the factor analysis, the path analysis results were compared by tundra and forest, permafrost, and vegetation differences. Figure 16 shows the distribution of path analysis

regression coefficients for tundra, forest, and non-permafrost forest sites for the daily (left) and weekly (right) timescales. Windspeed has the highest regression coefficient in all categories with tundra having the lowest median regression coefficients. The non-permafrost forest sites have a large range of windspeed coefficients on the daily timescale with the lower 1.5 interquartile range dipping slightly negative. On the daily scale, temperature has the second highest regression coefficient for all categories. Both ground heat flux and temperature have relatively high regression coefficients on the weekly scale for forest sites.

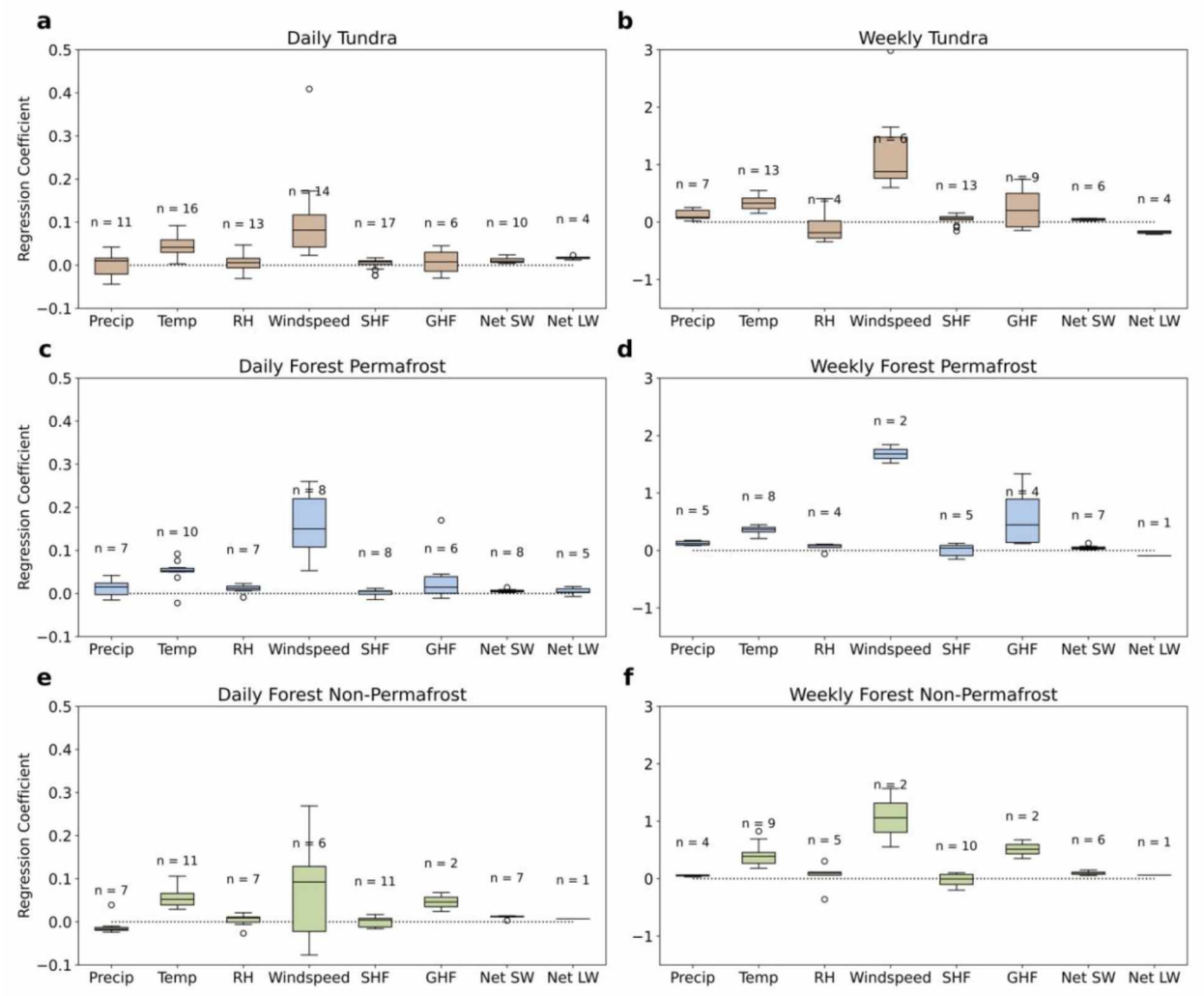

Figure 16. Distributions of regression coefficients for tundra (brown), boreal forest with permafrost (blue), and non-permafrost boreal forest (green) at the daily (left) and weekly (right) scales. Orange lines are median values, boxes represent interquartile range, and whiskers 1.5 times the interquartile ranges. Open circles are statistical outliers. Sample sizes are given for each variable.

Separating the path analysis results by permafrost shows several key differences in permafrost status consistent between forest and tundra sites. Figures 17 and 18 show the path analysis regression coefficients for tundra and forest sites, respectively, separated into continuous, discontinuous, and non-permafrost sites. Windspeed had the largest regression coefficient for all permafrost types in both the forest and tundra with distinctly higher

coefficients for discontinuous permafrost sites. Non-permafrost forest sites have the largest range of windspeed regression coefficients with both positive and negative values. Temperature has the second highest coefficient; however ground heat flux has a similar regression coefficient for the forest non-permafrost sites. The continuous permafrost sites show the least differences in regression coefficients between variables for both forest and tundra sites.

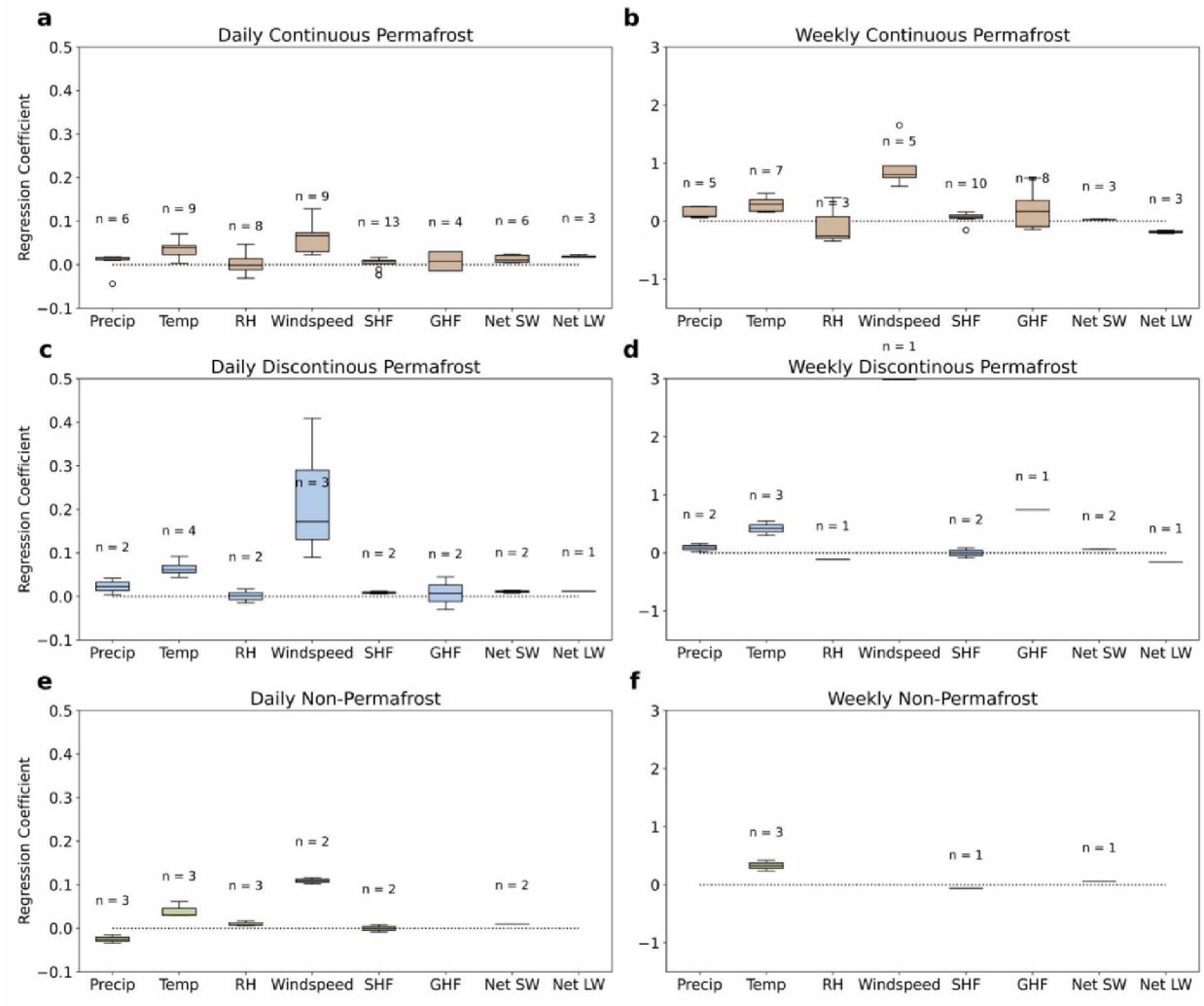

Figure 17. As in Figure 16, but for tundra sites with continuous permafrost (brown), discontinuous permafrost (blue), and non-permafrost (green).

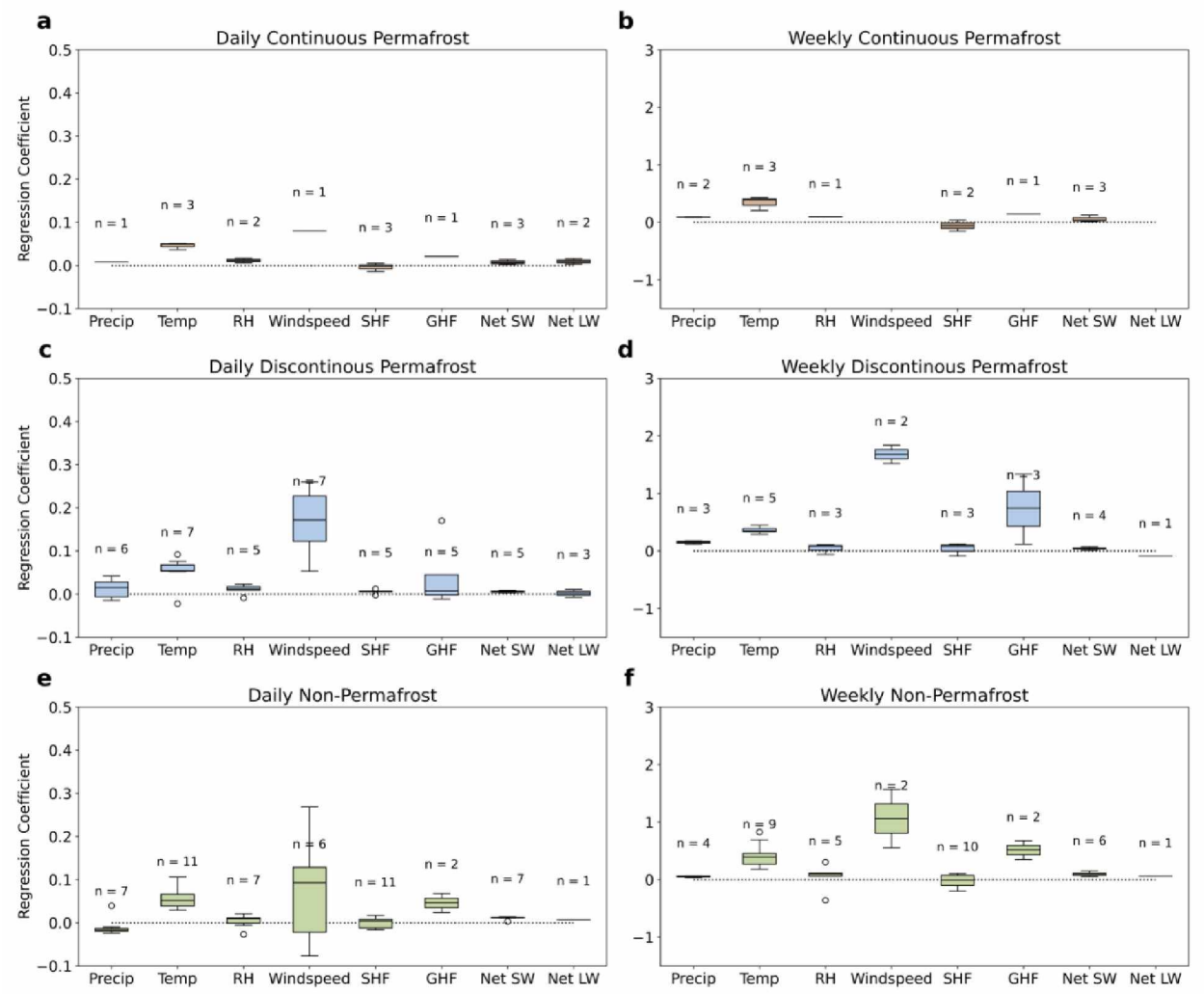

Figure 18. As in Figure 16, but for boreal forest sites with continuous permafrost (brown), discontinuous permafrost (blue), and non-permafrost (green).

Tundra and forest sites were separated by vegetation types in Figures 19 and 20 for the final comparisons of the path analysis. In the tundra shrubland and wetland sites windspeed continues to stand out with the highest regression coefficient, however this relationship does not appear in the grassland sites. There is no variable with a significantly larger regression coefficient than others for the grassland sites. In both tundra shrubland and wetland sites, temperature has the second highest regression coefficient for all timescales. However, ground heat flux has the largest range of regression coefficients for shrubland sites at the weekly

timescale. Most forest sites fall under the evergreen needleleaf vegetation, showing windspeed with the highest regression coefficient and largest range. Temperature is the second highest regression coefficient; however ground heat flux becomes similar to temperature in magnitude. Although the sample size is low for the other forest vegetation types, windspeed continues to have the highest regression coefficient with the highest coefficients at the wetland sites.

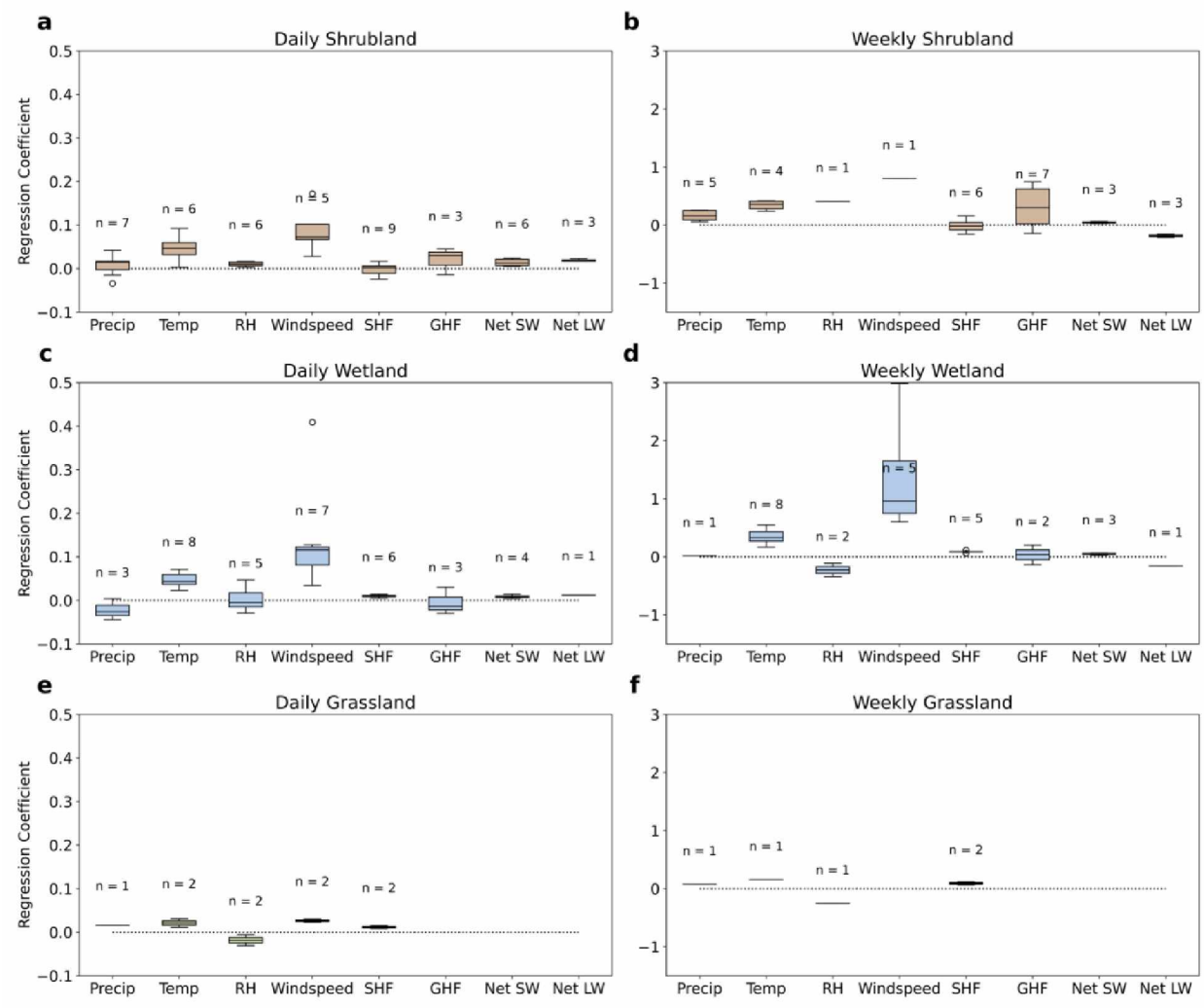

Figure 19. As in Figure 16, but for tundra sites in open shrubland (brown), wetland (blue), and grassland (green) vegetations.

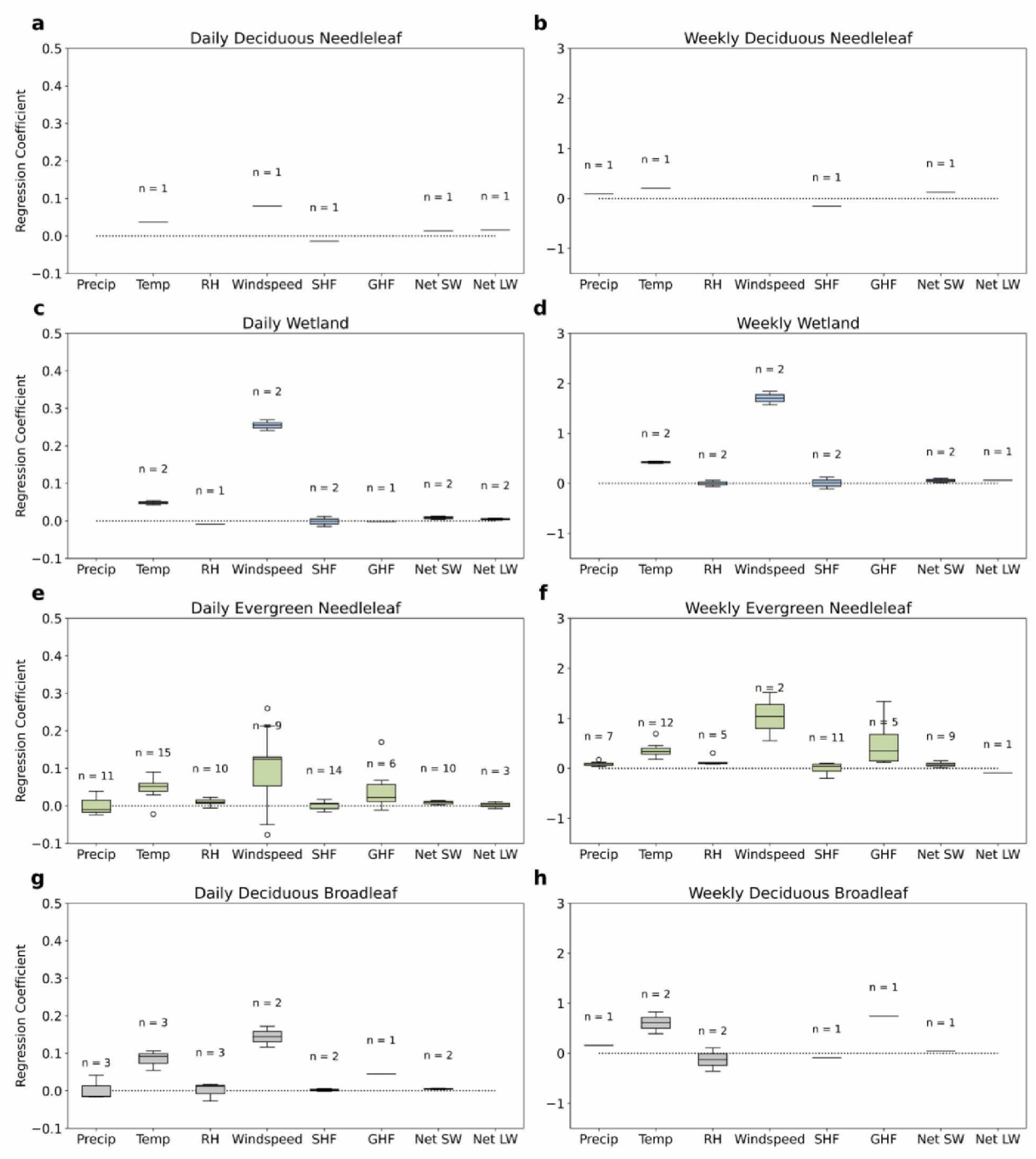

Figure 20. As in Figure 16, but for forest sites in deciduous needleleaf (brown), wetland (blue), evergreen needleleaf (green), and deciduous broadleaf (gray) vegetations.

To test the significance of differences in the regression coefficients of different variables in the path analysis, a Kruskal-Wallis test was run for all categories in Section 3.4 over all

variables. Results from the Kruskal-Wallis tests are shown in tables A4 - A6 in the appendix. All sites showed significant ($p \leq 0.05$) differences between variables for both daily and weekly timescales. The categories which showed significant differences in regression coefficients on all timescales for all variables are: tundra, forest permafrost, forest non-permafrost, forest evergreen needleleaf, tundra shrubland, tundra wetland, forest discontinuous permafrost, and tundra continuous permafrost. In comparison, the tundra discontinuous and non-permafrost, forest continuous permafrost, tundra grassland, forest wetland, forest deciduous needleleaf, and forest deciduous broadleaf categories showed no significant differences between variables on all timescales. The Kruskal-Wallis test does not give information on which variables show significant differences, so the test was performed twice more including only the temperature and ground heat flux variables, with another test also including windspeed. Only the daily runs of all sites, tundra, and tundra wetland showed significant differences between temperature and ground heat flux. When windspeed was included, significant differences were found for the previous categories as well as tundra continuous permafrost, forest discontinuous permafrost, and forest permafrost. This indicates that windspeed is a significant contributor to ET variability for the sites where significant differences were found when windspeed was added.

Throughout the path analysis, windspeed had the largest regression coefficient onto ET, while the factor analysis found windspeed to have low loadings onto the first factor which explained approximately 50% of the variability in ET. To quantify the extent of influence windspeed has on ET, multiple regressions were run for the same sites and variables as the path analysis. Table A10 and A11 show the explained variance from multiple regressions with and without windspeed, as well as the percentage of contribution from windspeed to the total variability. This is calculated as the difference in the two explained variances divided by the total

variance. The average total variance in ET on the daily timescale is 0.58 with a standard deviation of 0.21. The contribution from windspeed is 1.19% with a standard deviation of 1.94%. At the weekly scale, the average total variance is 19.0 with a standard deviation of 6.75, and the average contribution from windspeed is 0.71% with a standard deviation of 0.92%. Therefore, the actual contributions from windspeed to the total are low even though windspeed appears to have the largest independent influence on ET in the path analysis.

4. Discussion

4.1 Seasonal and Interannual Surface Moisture

Total annual P has a much larger interannual variability than total annual ET between all the sites, consistent with Brümmer et al.'s (2012) finding that total annual ET was only slightly affected by P across a network of boreal forest, peatland and grassland sites of Canada. Brümmer et al. also found that temperature, growing season length, and vegetation type were not strongly related to climatological mean values of annual ET.

The seasonality of surface moisture budget components varies across vegetation and permafrost status. Boreal forest sites underlain by permafrost show a distinct seasonal cycle of P-ET, with moisture deficits in the late spring and early summer. This systematic drying during May-June is not apparent at the tundra sites, although nearly half the tundra sites have negative P-ET in June. One reason for the absence of prominent drying at the tundra sites is the later snowmelt in the tundra, which generally delays the start of the growing season (and transpiration) until mid-June (Raz-Yaseef et al., 2017). The shorter growing season and the

smaller amounts of precipitation limit both the magnitudes and the duration of substantial interannual variations at the tundra sites in comparison to the forest sites.

Between the boreal forest sites, the non-permafrost sites receive more P and have a larger ET than the permafrost sites, especially in May and June. The resulting P-ET for these sites shows a moisture deficit for permafrost sites where the non-permafrost sites have a neutral and slight increase in moisture for these months. The conclusion is that the increased P outweighs the increased ET at the non-permafrost sites. The boreal forest non-permafrost sites are wetter in the sense that they receive more P and have larger P-ET than the boreal forest sites with permafrost. The median values of P-ET are well above zero from October through February and median values are close to zero in the spring months. The fact that these sites receive more precipitation than the Arctic sites partially explains the tilt towards their wetter (larger P-ET) surface moisture budgets. This positive net flux corresponds to the annual mean runoff if the long-term changes in soil moisture are small. The net gain of moisture from the atmosphere also contrasts with early estimates of the surface moisture imbalance, which indicate a net loss of surface moisture to the atmosphere (Newman and Branton, 1972).

At all the sites on which Figure 3 is based, a winter snowpack overlies a frozen ground surface during the winter months. During spring, most of the melted snow water flows towards rivers as surface runoff because the soil surface is still frozen, resulting in a minimal contribution of winter snowfall to the soil moisture. On the other hand, the preceding autumn's precipitation infiltrates the ground, although only in the active layer where permafrost is present, and is frozen into the upper soil layers during winter. During the spring melt season, this water is available for

ET. Greater soil moisture availability at the non-permafrost boreal forest sites provides one explanation for the absence of a soil moisture deficit in the spring (Figure 3c). Relative to the boreal forest permafrost sites, the boreal forest non-permafrost sites also have greater interannual variability in most calendar months. The interannual variability of autumn precipitation, which penetrates deeper into the soil column at the non-permafrost sites, may contribute to the greater range of interannual variations of P-ET at the non-permafrost sites. These conclusions about the interannual variability are subject to the caveat that the sample sizes are small (n = 5 for the permafrost forest sites and n = 3 for the non-permafrost forest sites).

Another consideration in the springtime moisture budget of boreal evergreen forest sites is the moisture limitation arising from frozen soil during the spring months when the soil is still frozen but trees have their needles and are ready for transpiration and growth. The evergreen spruce trees can use water stored in the sapwood for transpiration for several weeks before the soil thaws. But, after this water stored in the sapwood is used up, transpiration essentially stops and the trees are then moisture-limited (Tanja et al., 2003). However, this limitation will generally be present whether or not permafrost is present because seasonal freezing of the upper soil column occurs even without permafrost. Unless the roots extend well below the seasonally frozen layer, a springtime moisture limitation will still arise.

While most of the boreal forest sites show a positive annual water balance, other studies have found that the sign of the water balance can vary even among boreal forest sites in the same general region. For example, Sabater et al. (2019) studied two mountain birch forest sites in Fennoscandia and found a positive annual water imbalance at one site and a negative imbalance

at the other. This type of inter-regional variability is supported by the results presented here in the appendix. Another complication in the diagnosis of differences in the annual mean water balance is the partition of ET between evaporation and transpiration. In a study based on 65 boreal and arctic eddy covariance sites, including many used in this study, Kasurinen et al. (2014) showed that ET in wetlands and tundra occurs mostly from open water and ground evaporation, whereas ET in boreal forests is largely controlled by transpiration.

The sampling period and the possibility of temporal trends must also be considered in comparisons with previous studies. The results for Yakutsk provide an illustrative example. The overall net water balance range at the Yakutsk site was found here to be small compared to the other sites. In a similar analysis by Ohta et al. (2008) for the Yakutsk site using data from 1996-2008, the annual precipitation ranged from 111-347 mm $year^{-1}$ and the annual ET ranged from 169-220 mm $year^{-1}$. The data used in the present study based on data from 2012-2014 show annual precipitation ranging 260-345 mm $year^{-1}$ and annual ET ranging 293-300 mm yr^{-1}. The ranges of both variables are smaller than in Ohta et al.'s study, but ET is approximately 70 mm greater than Ohta et al.'s maximum value. Overall the annual precipitation at Yakutsk is small compared to other sites in the present study. However, consistent with the other sites, the interannual variability of P is greater than the interannual variability of ET at the Yakutsk site.

4.2 Sensitivity to Fire History

Disturbance by wildfire is a prominent feature of boreal ecosystems, with burn intervals at boreal forest locations ranging typically from several decades to a century. While the tundra also burns, the burn intervals are long, generally on the scale of centuries to millennia (Higuera et al., 2011). Based on our results for the Poker Flat site, the magnitude and duration of the mid-

year moisture deficits are directly related to the wildfire risk, as prolonged drying of surface vegetation favors the ignition by lightning (or humans) and spread of fires. The two years with the greatest moisture deficits (negative P-ET) were 2013 and 2015, both of which saw substantial acreage burned in Alaska. The early summer of 2015 was indeed warmer and drier than normal over much of Alaska, with departures from normal of about +2°C in temperature and -8% in relative humidity over the Poker Flat area (https://psl.noaa.gov/cgibin/data/composites/printpage.pl). The humidity deficit was even larger in northwest Alaska, although the temperature departures in that region were somewhat smaller than at Poker Flat. Approximately 5 million acres burned in Alaska during the summer of 2015, which was the year with Alaska's third largest burn area on record (Thoman and Walsh, 2019). By contrast, only about one million acres burned in 2013, largely because the surface moisture deficit was not as large as in 2015 during the crucial fire months of June and July. The 2013 moisture deficit was greatest in the late summer (August-September).

While wildfire can be associated with interannual variations of the surface moisture budget through their common association with hot and dry weather, there are also impacts of wildfire on surface fluxes. The variations of carbon fluxes during the recovery from a wildfire at black spruce forest sites have been evaluated by Ueyama et al. (2019). While the burn area was found to be a source of carbon in the year or two immediately following the wildfire, CO_2 emissions decreased during the plant succession over the following 5-10 years. By the second decade of recovery, the ecosystem had become a weak sink of CO_2. Leaf area index was found to be a key metric of the recovery of the carbon exchanges between the vegetation and the atmosphere. Although the impacts of wildfire on evapotranspiration has received less attention,

one may reasonably expect wildfire to impact the partitioning of evaporation and transpiration, and perhaps the total ET, as the plant succession follows a loss of vegetation.

Our results indicate that there is a detectable signal in the upward surface moisture flux (ET) for a period of several years to a decade following a wildfire. At the Poker Flat burn site in the boreal forest, the increase in ET as plant biomass has increased suggests that transpiration and reduced runoff contribute to the increased fluxes of moisture to the atmosphere during June and July for a period of about seven years (Figure 5). However, there is no increase of ET over the final three years in June, July or August, which are the months that provide the greatest contributions to the annual total ET (Figure 4). The fact that the post-fire increase of ET is limited to less than a decade is consistent with the recovery time of the CO_2 flux at the same site in the measurements of Ueyama et al. (2019).

The measurements from the burned and unburned areas of the Anaktuvuk tundra site provide an opportunity to assess the impact of wildfire disturbance on a tundra biome. An outstanding feature of Figure 5 is the series of anomalously high values during the first three years. The enhanced ET values are especially apparent in June at both the severe and moderate burn sites. The linear trends over the 12-year period are negative at both burn sites in all three months. These negative trends are statistically significant for five of the six month-burn-site combinations. By contrast, the trends are insignificant at the unburned site in all three months, pointing to an enhancement of ET in the fire scar in the first several years of the recovery. While the ET at the burn sites returns to the level of the unburned site in all three calendar months, the recovery time is somewhat longer in August than in June and July, when there is little trend in the burned areas after the first three years. The increase in ET for the first several years has been linked to an increase in evaporation from loss of the spongy moss and organic layer resulting in

surface water pooling and increased soil temperatures at the burned sites (Rocha et al., 2011). The increased soil temperatures, in turn, are consistent with the lower albedo of the fire scar during the period prior to vegetative recovery. After these initial years, ET follows the more typical post-fire decrease in latent heat flux consistent with a decrease in leaf area and transpiration (Rocha et al., 2011, Chambers et al., 2002, Amiro et al., 2006, Liu et al., 2008).

4.3 Factor Analysis

The results from the factor analysis show strong positive correlations between ET, temperature, sensible heat flux, ground heat flux, and net shortwave radiation for both boreal forest and tundra sites. These variables all display a strong seasonal cycle increasing in magnitude over the warm season, peaking around July. Net shortwave radiation is the primary driver of these seasonal cycles with the strong correlations shown in Figure 7. Within the connected seasonal cycles, the high sensible heat flux loadings are consistent with an excess of available surface energy during episodes of increased ET. Positive loadings with solar radiation and negative loadings with relative humidity are also consistent with warm and dry conditions during periods of enhanced ET (Liljedahl et al., 2011; Nazarbakhsh et al., 2019). Interestingly, wind speed and precipitation are less important relative to the other drivers on the shorter timescales, the implication is that the thermal drivers dominate the daily variations of ET.

With regard to the drivers, solar radiation is implicated as a key driver of evapotranspiration through its high loading on the multivariate factor that explains the most variance of ET. Because solar radiation is also a major driver of temperature in the lower atmosphere as evidenced by the diurnal cycle, it may also be presumed to contribute to variations in the downwelling longwave radiation that impacts the surface temperature. Similarly, the high loadings of the surface-atmosphere sensible heat flux at both the forest and tundra sites are

attributable, at least in part, to the linkage between incoming solar radiation and ground temperature. Variations of solar radiation at the ground surface are strongly dependent on variations in cloudiness, which in turn is positively correlated with precipitation. Reduced cloudiness can therefore favor drying through (a) an increase in net surface radiation, temperature and ET and (b) a reduction in P, both of which favor negative anomalies of P-ET.

It is notable that the relative humidity is one of the factors loading most heavily in the first factor for the boreal forest sites with a lower loading at tundra sites. The opposite signs of the ET and RH loadings in Figure 8 indicate that ET increases as relative humidity decreases, consistent with the bulk transfer formulations used in many climate models (e.g., Trenberth, 2010). Various studies have found strong correlations between ET and vapor pressure deficit (VPD) in boreal forest ecosystems. For example, Sabater et al. (2019) showed that northern high-latitude woodland ecosystems are largely driven by VPD, radiation, and temperature. In particular, VPD was found to control the transpiration component of ET in birch forests. VPD is directly related to relative humidity, and findings from Brümmer et al. (2012), Dolman et al. (2004), Kosugi et al. (2007) and Ohta et al. (2008) show that ET is strongly controlled by VPD, consistent with the high loading factor for relative humidity seen in Figure 8.

Taken together, these results indicate that ET at the tundra sites are more temperature-limited than moisture limited. The stronger loadings of net shortwave radiation for tundra sites in Figure 8 reinforces the importance of the temperature, which is largely driven by solar radiation. Interestingly, the precipitation loadings for tundra sites are slightly negative for the daily data, although slightly positive for the monthly data. The positive loading of precipitation at the monthly timescale points to a possible linkage of precipitation to photosynthetic activity (hence increased transpiration) over several weeks following a precipitation event, while the

negative loadings at the daily and weekly scales imply an absence of an immediate impact of precipitation on evaporation and ET in general. The correlations presented in Figure 7 confirm that precipitation is of relatively minor importance as a driver of variations of ET.

The role of temperature on the overall variability of ET appears to have a relationship with permafrost. In both tundra and forest sites, temperature loads higher on the first factor with higher amounts of permafrost, one of the most distinguishing differences between the two ecosystems. Eugster et al. (2002) describes permafrost acting as a buffer in the energy partitioning into sensible and ground heat fluxes to influence surface air temperatures. This buffer can impact the responses of thermal variables such as temperature to increased solar radiation during the warm season. However, this mechanism appears to act opposite in the factor analysis used in this study. In areas with more permafrost, the variability in air temperature follows similar patterns to increased net solar radiation than in areas with less permafrost. This behavior is also seen in ET at tundra sites, with ET following more similar variability patterns as radiation and thermal variables for areas with more permafrost than those without. Understanding how these relationships connect together and affect ET variability is a crucial area for future research to accurately model and predict future soil moisture in the Arctic.

4.4 Path Analysis

While windspeed was not among the variables with similar variability patterns to ET in the factor analysis, it overwhelmingly shows the most influence on ET independent from other variables in the path analysis. In all comparisons of the path analysis results, windspeed stood out with both the largest regression coefficients on ET and the largest range in coefficients. Windspeed was not among the group of variables with high factor loadings in the factor analysis and does not follow a distinct seasonal cycle over the warm season in response to increased solar

radiation. Together, these results can be interpreted to conclude that windspeed has the largest independent influence on ET. These effects are more pronounced at boreal forest sites than tundra, with non-permafrost forest sites showing the largest variability. However, discontinuous permafrost sites in both boreal forest and tundra show the largest effects of windspeed on ET. Although sample size is low (2) for wetland forest sites underlain by no and discontinuous permafrost, windspeed stands distinctly above all other variables.

This overwhelming dependency on windspeed is unique. Zhang et al. 2015 evaluated atmospheric controls on ET at a station in north China using a path analysis. Zhang et al. 2015 used net radiation, air temperature, vapor pressure deficit, and wind speed to predict ET with specified covariances between every predictor variable. Wind speed was found to have the least both direct and indirect effect on ET with net radiation having the largest direct effect. The stations used in the present analysis are remote high-latitude and many are underlain by permafrost, while Zhang et al. 2015 examined a mid-latitude agricultural irrigation site.

Permafrost has a distinct effect on the differences between variables in the path analysis. In both boreal forest and tundra, continuous permafrost sites show small differences in regression coefficients between variables, while discontinuous and non-permafrost sites show more pronounced differences. The presence of permafrost has a damping effect on independent variable contributions to ET variability. Although the tundra lacks even coverage of non-permafrost sites and the boreal forest lacks continuous permafrost sites, the damping effect is seen in both ecosystems.

Second to windspeed, temperature and ground heat flux show the greatest effects on ET. Unlike windspeed, the temperature regression coefficients are relatively consistent between vegetation types, permafrost status, and timescale aside from the natural increase in coefficients

as timescale increases. This implies the individual effects of temperature are consistent across vegetation and permafrost and show little variability. Compared to the differences in the factor analysis temperature loadings by permafrost, the consistency seen in the path analysis further implies that the different factor loadings on temperature arise from associations with other variables such as solar radiation. Ground heat flux does not show this consistency: as the timescale increases, ground heat flux increases in relative importance at forest sites. On the weekly timescale ground heat flux becomes comparable to temperature in its regression coefficients. Ground heat flux has large diurnal variability as Purdy et al., 2016 describe, contributing to lower regression coefficients on the daily scale. This variability is smoothed by the longer timescales and the regression coefficient onto ET increases in response.

5. Conclusions

The results presented here document the variations of high-latitude evapotranspiration, with emphasis on the seasonal cycle, interannual variations, and driving variables. This analysis focused on measurements from boreal and tundra ecosystems representing a large range of permafrost and vegetation types. The key findings are the following:

- The surface moisture budget at boreal forest permafrost sites shows a generally consistent seasonal cycle, with moisture deficits in the late spring and early summer, followed by moisture surpluses from late summer into autumn, consistent with the seasonal increase in precipitation. The spring deficit of P-ET is not apparent at permafrost-free boreal forest sites. The annual mean surface moisture flux (P-ET) is positive at most of the boreal forest sites, consistent with a long-term balance achieved by runoff (assuming no change in soil moisture storage).

- Tundra sites show a similar but less distinct seasonal cycle of P-ET than the boreal sites, with positive and negative net fluxes in all calendar months. There is a net gain of moisture in the annual mean at the tundra sites.
- Boreal forest sites in non-permafrost areas also show greater interannual variation in the monthly net surface moisture flux, and the net annual gain (P-ET) is larger than at the tundra and boreal forest sites underlain by permafrost.
- Interannual variability of the yearly net moisture gain is large at the boreal forest sites, ranging from about 3 cm to more than 30 cm at the Poker Flat black spruce supersite. The years with the largest mid-year deficits tend to be the years with the largest areas burned by wildfires in Interior Alaska.
- Measurements from a burned boreal forest site in interior Alaska show an increase in evapotranspiration over the decade following the fire. By contrast, the increase at a burned tundra site is limited to only a few years, after which ET decreases. In both cases, there is a short-term increase of ET relative to a nearby unburned site.
- Net solar radiation drives most of the shared variability and seasonal cycles of ET, temperature, sensible heat flux, ground heat flux, and net longwave radiation.
- Overall variability in ET at forest sites shows a stronger dependence on relative humidity while ET at tundra sites depends more strongly on air temperature and thermal variables.
- Windspeed has the largest independent contribution to ET variability. Although sample size is low, windspeed stands distinctly above all other variables for wetland forest sites.

The large interannual variability in P-ET is relevant to wildfire activity, as indicated by the large P-ET deficits during severe fire years at the Poker Flat black spruce forest site (Figure 4). This variability represents an opportunity and a challenge in seasonal prediction. While

precipitation is obviously an essential consideration in forecasts of P-ET, the results presented here also show that several variables can be viewed as proxies for ET. A leading candidate for useful skill in this regard is air temperature, which is a routinely released product of seasonal prediction centers. Largely because the skill of forecasts of key ET drivers such as wind speed, solar radiation, and relative humidity has not been demonstrated, these variables are typically not included in the suite of products of most forecasting centers. The results obtained here suggest that any such products that contain even modest skill would be useful for anticipating dry or wet states of the high-latitude land surface during the warm season, hence the predisposition of the landscape for wildfire. In terms of unique information (i.e. independent of the other variables), the path analysis showed that wind speed should be a consideration in forecasts of ET and associated surface drying.

Finally, the results presented here are based on point data from a limited number of local measurement sites. For example, the conclusion that tundra ET is temperature-limited while boreal ET has stronger dependencies on relative humidity is based on approximately 45 tundra locations and boreal forest sites with roughly equal representation for the two categories. These sites consist of a mix of vegetation types, soil types, topographic influences, and the presence or absence of permafrost. All these factors can be expected to influence ET and the net surface moisture balance. Moreover, these sites have varying record lengths that are generally subject to the vagaries of funding. While the archives of networks such as AmeriFlux and FLUXNET provide quality-controlled data from many of the eddy covariance sites, there are sufficient temporal and spatial gaps that alternative sources of information are needed for spatially comprehensive analyses to confirm the types of conclusions obtained here. Furthermore, not all

eddy covariance sites in this region have been included in these databases, and if they are, the most recent data are not always available (e.g., Helbig et al., 2020). Remote sensing and climate models have the potential to be such sources, although they require the *in situ* data described here for validation and calibration. The polar regions present some unique challenges in this regard, as permafrost complicates the application of terrestrial models and the high latitudes limit routine remote sensing to polar-orbiting satellites. The relationships obtained here between P, ET and their drivers must be captured if ET results from model simulations and remote sensing are to be considered realistic.

Acknowledgments

This work was supported by the National Science Foundation, Office of Polar Programs, through Grant ARC-1830131. Adrian Rocha's contribution was supported by the National Science Foundation, Division of Environmental Biology, through Grant No.: 1556772.

References

Amiro, B.D., et al., 2006. The effect of post-fire stand age on the boreal forest energy balance. *Agricultural and Forest Meteorology*, **140**, 41-50, https://doi.org/10.1002/2015JG003131.

Avis, C.A., et al., 2011. Reduction in areal extent of high-latitude wetlands in response to permafrost thaw. *Nature Geosciences*, **4**, 441-448, https://doi.org/10.1038/ngeo1160.

Bintanja, R., Selten F.M., 2014. Future increases in Arctic precipitation linked to local evaporation and sea-ice retreat. *Nature*, **509**, 479-482, https://doi.org/10.1038/nature13259.

Bring, A., et al., 2016. Arctic terrestrial hydrology: A synthesis of processes, regional effects, and research challenges. *Journal of Geophysical Research: Biogeosciences*, **121**, 621-649, https://doi.org/10.1002/2015JG003131.

Brümmer, C., et al., 2012. How climate and vegetation type influence evapotranspiration and water use efficiency in Canadian forest, peatland and grassland ecosystems. A*gricultural and Forest Meteorology*, **153**, 14-30. https://doi.org/10.1016/j.agrformet.2011.04.008.

Chambers, S.D., Chapin III F.S., 2002. Fire effects on surface-atmosphere energy exchange in Alaskan black spruce ecosystems: Implications for feedbacks to regional climate, *Journal of Geophysical Research Atmospheres*, **107**, 8145-8161, https://doi.org/10.1029/2001JD000530.

Confirmatory Factor Analysis (CFA) in R with Lavaan. From https://stats.idre.ucla.edu/r/seminars/rcfa/#s2

Destouni, G., Verrot, L. 2014. Screening long-term variability and change of soil moisture in a changing climate. *Journal of Hydrology*, **4**, 131-139, https://doi.org/10.1016/j.jhydrol.2014.01.059.

Dolman, A.J., et al., 2004. Net ecosystem exchange of carbon dioxide and water of far eastern Siberian Larch (Larix cajanderii) on permafrost. *Biogeosciences*, **1**, 133-146, https://doi.org/10.5194/bg-1-133-2004.

Eugster, W., et al., 2002. Land-atmosphere energy exchange in Arctic tundra and boreal forest: available data and feedbacks to climate. *Global Change Biology*, **6**, 84-115, https://doi.org/10.1046/j.1365-2486.2000.06015.x

Helbig, M., et al., 2020. Increasing contribution of peatlands to boreal evapotranspiration in a warming climate. *Nat. Clim. Chang.* **10**, 555–560, https://doi.org/10.1038/s41558-020-0763-7

Hinzman, L.D., et al., 2013. Trajectory of the Arctic as an integrated system. *Ecological Applications*, 23, 1837-1868, https://doi.org/10.1890/11-1498.1.

Introduction to Structural Equation Modeling (SEM) in R with Lavaan. UCLA: Statistical Consulting Group. From https://stats.idre.ucla.edu/r/seminars/rsem/

IPCC, 2013: Climate Change 2013. *The Physical Science Basis*. Report of Working Group I of the Intergovernmental Panel on Climate Change. Cambridge University Press, Cambridge, U.K.

Kasurinen, V., et al., 2014. Latent heat exchange in the boreal and arctic biomes. *Global Change Biology*, **20**, 3439-3456, https://doi.org/10.1111/gcb.12640.

Kosugi, Y., et al., 2007. Evapotranspiration over a Japanese cypress forest. I: Eddy covariance fluxes and surface conductance characteristics for 3 years, *J. Hydrology*, **337**, 269-283, https://doi.org/10.1016/j.jhydrol.2007.01.039.

Krupnik, I., and Jolly D., 2002. *The Earth is Faster Now: Indigenous Observations and Arctic Environmental Change*. Arctic Research Consortium of the United States, Fairbanks, Alaska, USA, 384 pp., ISBN 0-9720449-0-6.

Kruskal, W., and Wallis A., 1952. Use of Ranks in One-Criterion Variance Analysis. *Journal of the American Statistical Association*, **47**, 583-621, https://doi.org/10.2307/2280779.

Liljedahl, A.K., et al., 2011. Nonlinear controls on evapotranspiration in Arctic coastal wetlands. *Biogeosciences*, **8**, 3375-3389, https://doi.org/10.5194/bg-8-3375-2011.

Liu, H., Randerson J., 2008. Interannual variability of surface energy exchange depends on stand age in a boreal forest fire chronosequence. *Journal of Geophysical Research Biogeosciences*, **113**, G01006, https://doi.org/10.1029/2007JG000483.

Nazarbakhsh, M., et al., 2019. Controls on evapotranspiration from jack pine forests in the boreal plains ecozone. *Hydrological Processes*, **34**, 927-940, https://doi.org/10.1002/hyp.13674.

Newman, J.E., Branton C.I., 1972. Annual water balance and agricultural development in Alaska. *Ecology*, **53**, 513-519, https://doi.org/10.2307/1934243.

Ohta, T., et al., 2008. Interannual variation of water balance and summer evapotranspiration in an eastern Siberian larch forest over a 7-year period (1998-2006). *Agricultural and Forest Meteorology*, **148**, 1941-1953, https://doi.org/10.1016/j.agrformet.2008.04.012.

Pastorello, G., et al., 2020. The FLUXNET2015 dataset and the ONEFlux processing pipeline for eddy covariance data. *Scientific Data*, **7,** 225, https://doi.org/10.1038/s41597-020-0534-3.

Purdy, A.J., et al., 2016. Ground Heat Flux: An analytical review of 6 models evaluated at 88 sites and globally. *Journal of Geophysical Research: Biogeosciences,* **121**, 3045-3059, https://doi.org/10.1002/2016JG003591.

Raz-Yaseef, N., et al., 2017. Evapotranspiration across plant types and geomorphological units in polygonal Arctic tundra. *Journal of Hydrology*, **533**, 816-825, https://doi.org/10.1016/j.jhydrol.2017.08.036.

Rocha, A., Shaver G., 2011. Postfire energy exchange in arctic tundra: the importance and climatic implications of burn severity. *Global Change Biology*, **17**, 2831-2841, https://doi.org/10.1111/j.1365-2486.2011.02441.x

Sabater, A.M., et al., 2019. Transpiration from subarctic deciduous woodlands: Environmental controls and contribution to ecosystem evapotranspiration. *Ecohydrology*, **13**, e2190, https://doi.org/10.1002/eco.2190.

Tanja, S., et al., 2003. Air temperature triggers the recovery of evergreen boreal forest photosynthesis in spring. *Global Change Biology*, **9**, 1410-1426, https://doi.org/10.1046/j.1365-2486.2003.00597.x.

Thoman, R., J. E. Walsh, 2019. Alaska's changing environment: documenting Alaska's physical and biological changes through observations. H. R. McFarland, Ed. International Arctic Research Center, University of Alaska Fairbanks.

Ueyama, M., et al., 2019. Carbon dioxide balance in early-successional forests after forest fires in interior Alaska. *Agricultural and Forest Meteorology*, **275**, 196-207, https://doi.org/10.1016/j.agrformet.2019.05.020.

USGCRP, 2017: *Climate Science Special Report: Fourth National Climate Assessment*, Volume I[Wuebbles, D.J., D.W. Fahey, K.A. Hibbard, D.J. Dokken, B.C. Stewart, and T.K. Maycock (eds.)]. U.S. Global Change Research Program, Washington, DC, USA, 470 pp, doi: 10.7930/J0J964J6.

Zhang, B., et al., 2015. Multi-scale evapotranspiration of summer maize and the controlling meteorological factors in north china. *Agricultural and Forest Meteorology*, **216**, 1-12, https://doi.org/10.1016/j.agrformet.2015.09.015.

Appendix

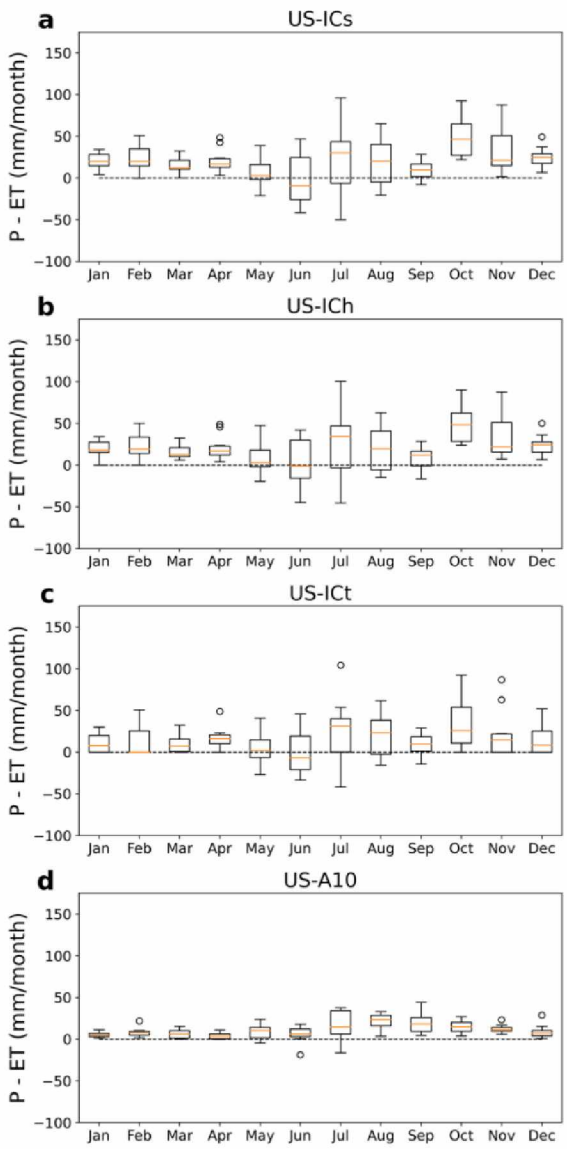

Figure A1: Distributions of total monthly precipitation – evapotranspiration difference for tundra sites (a) US-ICs Imnavait Creek fen, (b) US-ICh Imnavait Creek ridge, (c) US-ICt Imnavait Creek tussock, and (d) US-A10 Utqiagvik. Orange lines are median values, boxes represent interquartile range, and whiskers 1.5 times the interquartile ranges. Open circles are statistical outliers.

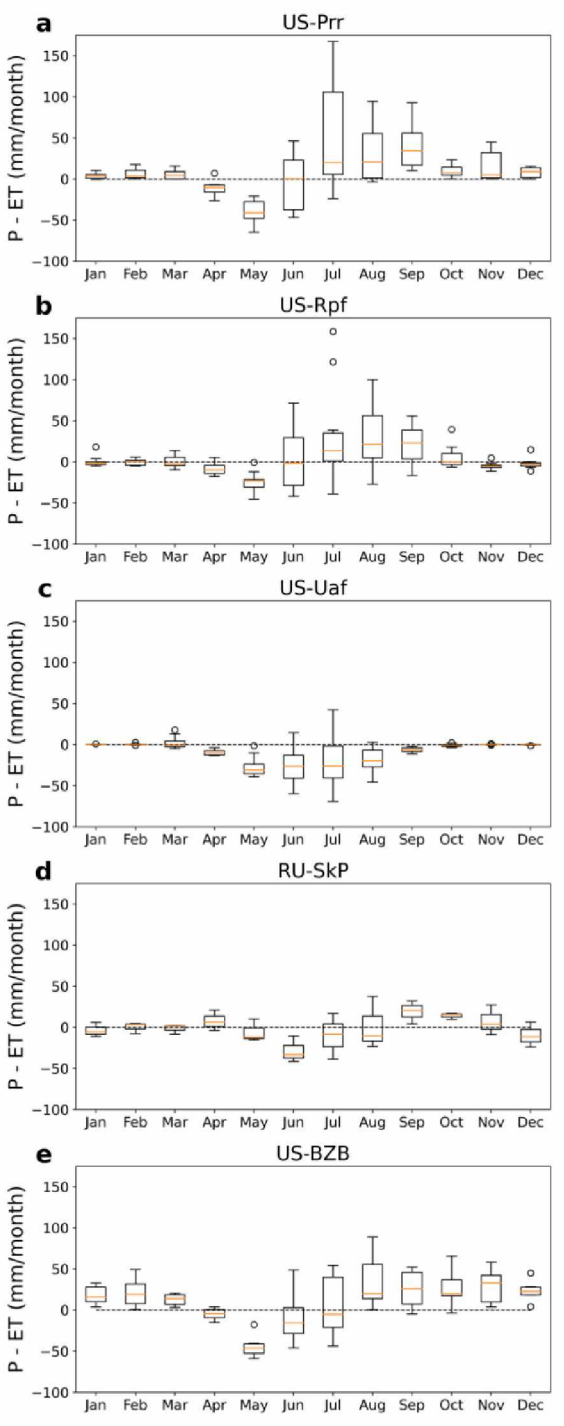

Figure A2: Same as Figure A1 but for boreal forest permafrost sites (a) US-Prr Poker Flat black spruce forest, (b) US-Rpf Poker Flat deciduous forest, (c) US-Uaf University of Alaska Fairbanks, (d) RU-SkP Yakutsk Spasskaya Pad, (e) US-BZB Bonanza Creek thermokarst.

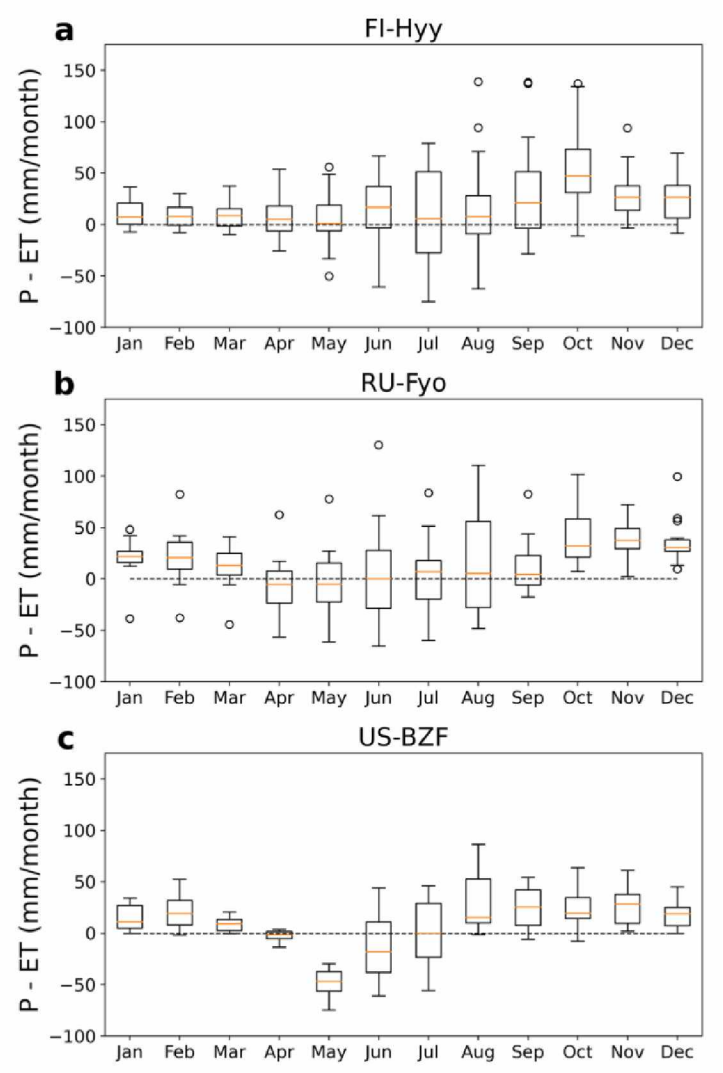

Figure A3: Same as Figure A1 but for boreal forest non-permafrost sites (a) FI-Hyy Hyytiala, (b) RU-Fyo Fyodorovskoye, and (c) US-BZF Bonanza Creek Fen.

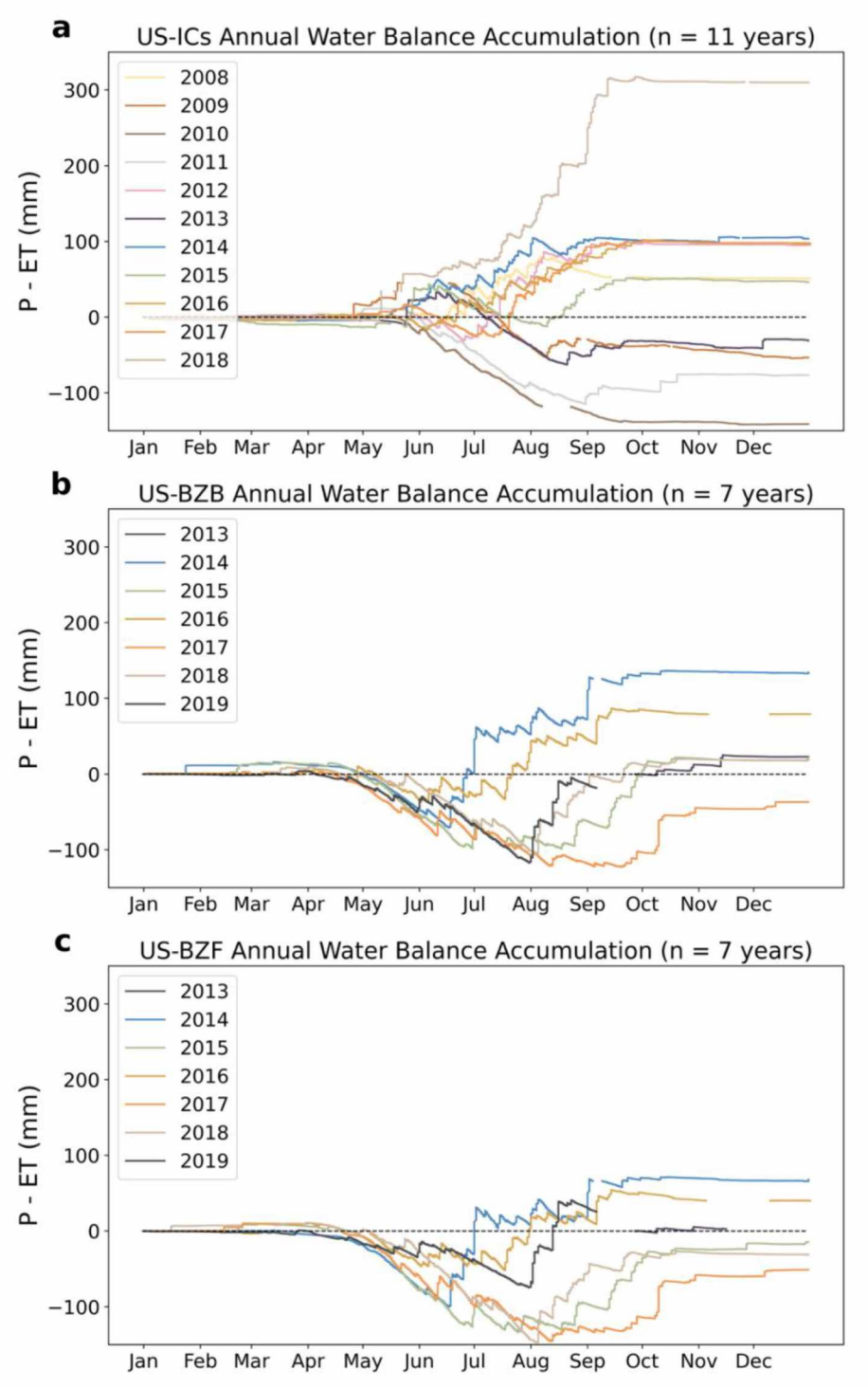

Figure A4: Yearly cumulative totals of P-ET at (a) US-ICs Imnavait Creek fen, (b) US-BZB Bonanza Creek thermokarst, and (c) US-BZF Bonanza Creek Fen. Years are color-coded according to legend in upper left corner.

Table A1: Daily regression coefficients and sample size for all path analysis sites. Non-significant values are in gray.

Site ID	Precip	Temp	RH	Windspeed	SHF	GHF	Net SW	Net LW	Sample Size
US-An2	0.013	0.005	0.013	0.059	-0.024	-0.009	0.023	0.017	196
US-An1	0.021	-0.025	0.016	0.04	-0.023	0.007	0.024	0.023	114
US-An3	0.018	0.016	0.003	0.067	-0.011	-0.008	0.016	0.017	189
US-Atq	-0.044	0.023	-0.029	0.128	0.005	0.03			676
US-BZS	0.008	0.051	0.006		0.005	0.021	0.002		1220
US-Bn1	0.033	-0.022	0.009	0.053	0.002	0.17	0.001		413
US-Bn2	0.042	0.092	0.017	0.172	0.006	0.045			384
US-Bn3	0.042	0.092	0.017	0.172	0.006	0.045			384
US-BZF	0	0.043	0.002	0.269	-0.015	-0.003	0.013	0.007	812
US-BZB	0.002	0.054	-0.009	0.241	0.012	-0.002	0.004	0.002	829
CA-Man	0.001	0.071		0.124	0.007				1768
CHET	-0.012	0.071		0.073	0.009				564
FI-Hyy	-0.01	0.09	-0.006		0.007				2327
FI-Var	-0.016			0.039	0.004	0.068			415
DK-NuF/GL-NuF	0.004	0.064	-0.015	0.09	0.012				969
DK-ZaF/GL-ZaF	-0.003	0.039	0.047		0.01				612
DK-ZaH/GL-ZaH	-0.002	0.031	-0.006	0.023	0.008				2295
US-ICs	0.008	0.044	-0.005	0.117	0.008	-0.002	0.004		1365
US-ICh	0.01	0.039	0.001	0.072	0.003	-0.003	0.006		1397
US-ICt	0.015	0.055	0.003	0.002	0.002	-0.014	0.005		1250
IS-Gun	-0.017	0.106	-0.027	-0.006	0		0.003		342
US-Rpf	-0.015	0.054	0.012	0.117	-0.002	0	0.007		1407
US-Prr	-0.013	0.052	0.002	0.128	0.007	0.008	0.003	-0.007	846
RU-Cok	0.017	0.003		0.028	0.017	0.03			1836
RU-Fyo	-0.018	0.061	0	0.13	0.01	0.024		0	2479
RU-Fy2	-0.024	0.058	0.021	0.006	-0.003	-0.005	0.012	0.003	500
RU-Sam	0.016	0.011	-0.031	0.03	0.015				1828
RU-SkP	0.021	0.037		0.08	-0.014	0.03	0.014	0.016	430
YPF	0.022	0.05	0.017	0.015	-0.002		0.007	0.003	412

Table A1, Continued.

RU-Zot	-0.026	0.029	0.017	0.116	-0.004		0.009		253
CA-SCB	0.003	0.058	-0.005	0.409	-0.001	-0.03	0.014	0.012	479
CA-SCC	0.015	0.06	0.002	0.26	-0.001	-0.004	0.009	0.011	506
SE-Sk1	0.039	0.038		0.04	0.017				523
SE-St1	0.003	0.044	0.005	0.014	0.001		0.008		365
SJ-Adv	0.014	0		0.034	0.014	-0.014			437
US-Uaf	0.015	0.076	0.023	0.213	0.005	-0.011	0.005		1238
CA-NS1	0.009	0.037	0.01	0.061	-0.009		0.011		475
CA-NS2	-0.01	0.029	0.012	-0.05	-0.012		0.013		431
CA-NS3	-0.014			0.03	-0.016		0.014		565
CA-NS4	-0.003	0.04	0.004	-0.01	0.009				392
CA-NS5	-0.021	0.052	0.009	-0.077	-0.012		0.012		549
CA-NS6	-0.015	0.03	0.006	-0.008	-0.009		0.009		555
CA-NS7	-0.034	0.061	0.008	0.102	0.008				413

Table A2: Weekly regression coefficients and sample size for all path analysis sites. Non-significant values are in gray.

Site ID	Precip	Temp	RH	Windspeed	SHF	GHF	Net SW	Net LW	Sample Size
US-An2	0.102	-0.087	0.083	1.746	0.089	0.501	0	-0.19	38
US-An1	0.25	-0.325	0.41	-0.297	-0.155	0.741	0.031	-0.211	29
US-An3	0.254	0.209	0.131	-0.413	0.107	0.303	-0.034	-0.153	38
US-Atq	0.083	0.176	-0.342	1.653	-0.025	0.204			123
US-BZS	0.018	0.39	0.031		0.04	0.146	0.012		188
US-Bn1	0.088	-0.156	-0.046	-0.046	-0.008	1.335	-0.008		65
US-Bn2	0.159	0.324	0.013	0.687	-0.09	0.745			65
US-Bn3	0.159	0.324	0.013	0.687	-0.09	0.745			65
US-BZF	-0.004	0.4	0.061	1.57	-0.112	-0.031	0.101	0.063	126
US-BZB	0.009	0.448	-0.06	1.84	0.124	0.001	0.011	-0.008	129
CA-Man	0.064	0.458		0.554	0.043				289
CHET	0.011	0.476		0.75	0.061				81
FI-Hyy	0.033	0.692	-0.041		0.038				380
FI-Var	-0.007			0.639	-0.016	0.676			62
DK-NuF/GL-NuF	0.018	0.419	-0.111	0.576	0.089				140
DK-ZaF/GL-ZaF	-0.02	0.167	0.436		0.094				88
DK-ZaH/GL-ZaH	-0.001	0.154	-0.016	0.086	0.064				328
US-ICs	0.031	0.328	-0.035	0.955	0.087	-0.042	0.022		214
US-ICh	0.038	0.297	0.043	0.803	0.036	-0.083	0.04		219
US-ICt	0.059	0.412	0.029	0.035	0.048	-0.145	0.026		196
IS-Gun	0.05	0.826	-0.359	-0.551	-0.003		0.007		51
US-Rpf	-0.008	0.391	0.109	0.587	0.013	0.023	0.041		218
US-Prr	-0.023	0.333	0.025	2.16	0.086	0.119	-0.01	-0.093	125
RU-Cok	0.087	-0.018		-0.004	0.159	0.13			263
RU-Fyo	-0.009	0.389	0.114	0.405	0.087	0.352		0.01	359
RU-Fy2	-0.042	0.013	0.305	-0.567	-0.088	0.162	0.104	-0.092	72
RU-Sam	0.076	0.02	-0.255	0.071	0.12				265
RU-SkP	0.093	0.206		0.449	-0.154	0.278	0.125	0.077	64
YPF	0.083	0.431	0.095	-0.019	0.001		0.037	0.01	62
RU-Zot	0.043	0.329	0.043	0.926	0.01		0.024		45
CA-SCB	0.037	0.549	0.14	2.983	-0.064	-0.057	0.059	-0.154	77
CA-SCC	0.121	0.345	0.088	1.52	-0.089	0.048	0.071	-0.06	81
SE-Sk1	0.066	0.175		0.541	0.103				79
SE-St1	0.034	0.301	0.037	0.144	-0.016		0.065		55

Table A2, Continued.

SJ-Adv	0.049	-0.062		0.602	0.115	-0.135			63
US-Uaf	0.175	0.289	0.086	0.437	0.02	0.058	0.044		248
CA-NS1	0.036	0.268	0.051	0.189	-0.063		0.068		80
CA-NS2	0.054	0.251	0.031	-0.419	-0.048		0.056		82
CA-NS3	0.031			0.038	-0.199		0.151		94
CA-NS4	0.035	0.288	0.098	-0.598	0.1				66
CA-NS5	-0.011	0.182	0.073	-1.132	-0.142		0.115		89
CA-NS6	-0.024	0.236	0.056	0.394	-0.063		0.062		85
CA-NS7	-0.062	0.422	0.058	0.835	0.041				72

Table A3: Monthly regression coefficients and sample size for all path analysis sites. Non-significant values are in gray.

Site ID	Precip	Temp	RH	Windspeed	SHF	GHF	Net SW	Net LW	Sample Size
US-An2	-0.481	18.217	-10.232	-182.769	-2.354	-46.675	5.481	11.689	10
US-An1									
US-An3									
US-Atq	0.3	1.21	-1.541	9.98	-0.279	1.414			33
US-BZS	0.012	1.986	0.206		0.176	0.689	0.057		45
US-Bn1	0.251	-0.903	-0.229	2.722	-0.67	5.433	0.246		15
US-Bn2	0.414	1.976	-2.212	2.841	-1.226	2.07			15
US-Bn3	0.414	1.976	-2.212	2.841	-1.226	2.07			15
US-BZF	0.102	0.402	-0.293	-17.765	-0.853	-0.414	0.71	0.871	31
US-BZB	0.065	1.682	-0.066	0.1	0.041	0.288	0.188	-0.032	31
CA-Man	0.243	1.553		4.231	0.162				74
CHET	0.084	2.038		-0.899	0.38				19
FI-Hyy	0.066	3.639	-0.014		0.305				90
FI-Var	0.077			0.431	0.039	2.317			15
DK-NuF/GL-NuF	0.031	1.991	-0.404	2.288	0.378				32
DK-ZaF/GL-ZaF	-0.066	0.741	0.163		0.394				20
DK-ZaH/GL-ZaH	0.004	1.029	0.217	-1.95	0.214				75
US-ICs	0.045	2.094	0.134	-0.412	0.032	-0.778	0.218		50
US-ICh	0.039	2.193	0.406	-1.478	-0.218	-1.129	0.33		50
US-ICt	0.058	2.265	0.629	0.373	-0.178	-1.178	0.273		47
IS-Gun	0.095	2.374	-2.941	-12.888	-0.058		-0.05		13
US-Rpf	-0.004	1.93	0.452	-3	0.048	0.625	0.114		52
US-Prr	-0.018	0.882	0.485	-3.989	0.255	0.925	-0.085	-1.133	29
RU-Cok	0.147	-0.166		1.74	0.806	0.081			60
RU-Fyo	0.05	0.834	1.299	-10.786	0.585	2.947		0.087	85
RU-Fy2	-0.077	-8.759	4.067	-61.45	-1.693	3.271	0.879	-2.942	18
RU-Sam	0.269	-0.392	-1.4	0.005	0.536				63
RU-SkP	0.239	0.065		-27.882	-0.508	4.157	0.427	0.03	15
YPF	0.209	1.832	-0.163	5.694	0.039		0.014	-0.004	17
RU-Zot	0.472	1.884	-0.245	17.195	-0.939		0.461		13
CA-SCB	0.622	-0.745	-3.56	22.875	2.498	-3.465	0.146	1.947	19
CA-SCC	0.226	2.018	-2.333	-0.732	0.234	-2.378	0.454	2.663	19
SE-Sk1	0.151	-0.324		0.459	0.608				20
SE-St1	-0.029	1.109	0.073	-19.506	-0.066		0.237		14
SJ-Adv	0.151	-0.894		7.333	0.684	-0.928			15

Table A3, Continued.

US-Uaf	0.306	1.041	0.183	-14.088	0.061	-0.448	0.256		59
CA-NS1	0.119	0.123	0.405	-23.882	-0.398		0.443		19
CA-NS2	0.213	1.52	-1.657	-17.176	-0.075		-0.062		22
CA-NS3	0.141			-21.901	-0.508		0.546		23
CA-NS4	0.078	1.188	0.509	-5.914	0.447				15
CA-NS5	0.2	1.859	-1.204	-36.989	-0.245		0.13		22
CA-NS6	-0.032	0.891	-0.7	-10.793	-0.62		0.321		20
CA-NS7	0.247	1.249	0.253	-36.42	0.355				19

Table A4: Kruskal-Wallis test statistic (H-value) and p-values for all path analysis categories. All variable regression coefficients are included as the test distributions. Non-significant values are in gray.

	Test Statistic		P-Value	
	Daily	Weekly	Daily	Weekly
Tundra Permafrost Continuous	29.59	26.12	0	0
Tundra Permafrost Discontinuous	12.27	10.78	0.09	0.15
Tundra Non-Permafrost	12.96	3.2	0.07	0.87
Forest Permafrost Continuous	12.36	8.87	0.09	0.26
Forest Permafrost Discontinuous	22.02	19.35	0	0.01
Forest Non-Permafrost	26.65	28.14	0	0
Tundra Wetland	26.98	23.24	0	0
Tundra Shrubland	23.77	18.3	0	0.01
Tundra Grassland	5.93	3.2	0.55	0.87
Forest Evergreen Needleleaf	30.48	37.72	0	0
Forest Deciduous Needleleaf	4	3	0.78	0.89
Forest Deciduous Broadleaf	11.36	5.92	0.12	0.55
Forest Wetland	9.04	7.68	0.25	0.36
Tundra	50.42	39.29	0	0
Forest Permafrost	32.01	27.26	0	0
Forest Non-Permafrost	26.65	28.14	0	0
All Sites	98.21	87.2	0	0

Table A5: Kruskal-Wallis test statistic (H-value) and p-values for all path analysis categories. Temperature, ground heat flux, and windspeed regression coefficients are included as the test distributions. Non-significant values are in gray.

	Test Statistic		P-Value	
	Daily	Weekly	Daily	Weekly
Tundra Permafrost Continuous	5.99	10.48	0.05	0.01
Tundra Permafrost Discontinuous	5.38	3.2	0.07	0.2
Tundra Non-Permafrost	3	0	0.22	1
Forest Permafrost Continuous	3.2	1.8	0.2	0.41
Forest Permafrost Discontinuous	8.77	4.73	0.01	0.09
Forest Non-Permafrost	0.69	2.74	0.71	0.25
Tundra Wetland	10.85	10.5	0	0.01
Tundra Shrubland	4.11	2.54	0.13	0.28
Tundra Grassland	0	0	1	0
Forest Evergreen Needleleaf	3.07	3.47	0.22	0.18
Forest Deciduous Needleleaf	1	0	0.61	0
Forest Deciduous Broadleaf	4.29	0	0.12	1
Forest Wetland	3.6	2.4	0.17	0.3
Tundra	11.75	13.14	0	0
Forest Permafrost	11.95	4.8	0	0.09
Forest Non-Permafrost	0.69	2.74	0.71	0.25
All Sites	20.73	20.29	0	0

Table A6: Kruskal-Wallis test statistic (H-value) and p-values for all path analysis categories. Temperature and ground heat flux regression coefficients are included as the test distributions. Non-significant values are in gray.

	Test Statistic		P-Value	
	Daily	Weekly	Daily	Weekly
Tundra Permafrost Continuous	3.46	0.66	0.06	0.42
Tundra Permafrost Discontinuous	1.93	1.8	0.16	0.18
Tundra Non-Permafrost	0	0	1	1
Forest Permafrost Continuous	1.8	1.8	0.18	0.18
Forest Permafrost Discontinuous	1.12	0.56	0.29	0.46
Forest Non-Permafrost	0.35	0.22	0.55	0.64
Tundra Wetland	4.19	2.45	0.04	0.12
Tundra Shrubland	1.36	0	0.24	1
Tundra Grassland	0	0	1	0
Forest Evergreen Needleleaf	1.19	0	0.28	1
Forest Deciduous Needleleaf	0	0	0	0
Forest Deciduous Broadleaf	1.8	0	0.18	1
Forest Wetland	1.5	0	0.22	1
Tundra	4.59	0.59	0.03	0.44
Forest Permafrost	2.31	0	0.13	1
Forest Non-Permafrost	0.35	0.22	0.55	0.64
All Sites	7.77	0.26	0.01	0.61

Table A7: Daily factor loadings on the first factor for all factor analysis runs.

Site ID	ET	Precip	Temp	RH	Windspeed	SHF	GHF	Net SW	Net LW
US-An2	0.84	-0.09	0.65	-0.71	0.17	0.57	0.65	0.94	-0.83
US-An1	0.68	-0.02	0.54	-0.75	0.15	0.64	0	0.96	-0.9
US-An3	0.78	-0.07	0.65	-0.72	0.18	0.64	0.54	0.94	-0.84
US-Atq	0.69	-0.13	0.78	-0.75	-0.19	0.48	0.61	0	0
US-BZS	0.76	-0.21	0.72	-0.68	0	0.79	0.72	0.83	0
US-Bn1	0.46	-0.31	0.72	-0.78	0.15	0.8	0.78	0.79	0
US-Bn2	0.59	-0.24	0.83	-0.77	0.07	0.63	0.85	0	0
US-Bn3	0.59	-0.24	0.83	-0.77	0.07	0.63	0.85	0	0
US-BZF	0.88	-0.29	0.58	-0.82	0.18	0.42	0.68	0.96	-0.8
US-BZB	0.94	-0.32	0.62	-0.85	0.12	0.83	0.75	0.92	-0.85
CA-Man	0.9	-0.29	0.64	0	-0.16	0.64	0	0	0
CHET	0.98	-0.13	0.81	0	0.03	0.49	0	0	0
FI-Hyy	0.74	-0.43	0.43	-0.78	0	0.85	0	0	0
FI-Var	0.79	-0.32	0	0	-0.07	0.68	0.76	0	0
DK-NuF/GL-NuF	0.94	-0.46	0.48	-0.25	-0.22	0.84	0	0	0
DK-ZaF/GL-ZaF	0.85	-0.23	0.69	0	-0.37	0.86	0	0	0
DK-ZaH/GL-ZaH	0.87	-0.2	0.7	-0.12	-0.14	0.84	0	0	0
US-ICs	0.89	-0.06	0.83	-0.53	0.13	0.67	0.68	0.93	0
US-ICh	0.83	-0.05	0.84	-0.51	0.17	0.69	0.75	0.94	0
US-ICt	0.85	-0.06	0.84	-0.53	0.04	0.71	0.68	0.93	0
IS-Gun	0.78	-0.57	-0.16	-0.86	0.06	0.17	0	0.77	0
US-Rpf	0.81	-0.37	0.72	-0.73	-0.03	0.77	0.82	0.96	0
US-Prr	0.89	-0.46	0.54	-0.82	0.35	0.9	0.45	0.95	-0.87
RU-Cok	0.78	-0.13	0.2	0	0.05	0.8	0.58	0	0
RU-Fyo	0.61	-0.27	0.73	-0.73	-0.22	0.86	0.62	0	-0.47
RU-Fy2	0.68	-0.41	0.57	-0.82	-0.14	0.84	0.52	0.96	-0.89
RU-Sam	0.8	-0.22	0.51	-0.62	-0.16	0.58	0	0	0
RU-SkP	0.59	-0.44	0.65	0	-0.09	0.81	0.64	0.95	-0.8
YPF	0.37	-0.38	0.66	-0.75	-0.22	0.31	0	0.87	-0.52
RU-Zot	0.62	-0.44	0.49	-0.8	-0.1	0.87	0	0.93	0
CA-SCB	0.86	-0.27	0.6	-0.81	0	0.27	0.61	0.96	-0.84
CA-SCC	0.76	-0.28	0.62	-0.78	-0.1	0.76	0.63	0.96	-0.89
SE-Fla	0.68	0	0.39	-0.71	-0.21	0.86	0	0	0
SE-Sk1	0.87	-0.12	0.31	0	0.04	0.8	0	0	0
SE-St1	0.83	-0.34	0.38	-0.75	-0.19	0.82	0	0.97	0
SJ-Adv	0.65	-0.04	0.61	0	-0.02	0.94	0.4	0	0
US-Uaf	0.69	-0.14	0.64	-0.68	0.38	0.83	0.68	0.95	0
CA-NS1	0.72	-0.22	0.46	-0.83	-0.04	0.87	0	0.98	0
CA-NS2	0.55	-0.46	0.25	-0.86	-0.02	0.88	0	0.93	0
CA-NS3	0.62	-0.37	0	0	-0.09	0.92	0	0.99	0

Table A7, Continued.

CA-NS4	0.76	-0.58	0.25	-0.74	-0.19	0.86	0	0	0
CA-NS5	0.71	-0.52	0.36	-0.86	-0.07	0.79	0	0.98	0
CA-NS6	0.63	-0.53	0.26	-0.87	-0.09	0.83	0	0.97	0
CA-NS7	0.6	-0.55	0.34	-0.87	-0.09	0.78	0	0	0

Table A8: Weekly factor loadings on the first factor for all factor analysis runs.

Site ID	ET	Precip	Temp	RH	Windspeed	SHF	GHF	Net SW	Net LW
US-An2	0.88	0.22	0.67	-0.73	0.28	0.63	0.79	0.91	-0.83
US-An1	0.72	0.17	0.62	-0.81	0.18	0.62	0	0.91	-0.9
US-An3	0.83	0.25	0.74	-0.78	0.06	0.61	0.66	0.92	-0.85
US-Atq	0.71	0.01	0.82	-0.82	-0.2	0.54	0.64	0	0
US-BZS	0.79	-0.19	0.71	-0.72	0	0.82	0.82	0.79	0
US-Bn1	0.56	-0.33	0.71	-0.83	0.16	0.86	0.85	0.86	0
US-Bn2	0.55	-0.22	0.75	-0.84	0.15	0.74	0.94	0	0
US-Bn3	0.55	-0.22	0.75	-0.84	0.15	0.74	0.94	0	0
US-BZF	0.86	-0.32	0.52	-0.86	0.43	0.34	0.8	0.98	-0.81
US-BZB	0.93	-0.31	0.6	-0.89	0.41	0.89	0.85	0.95	-0.88
CA-Man	0.87	-0.01	0.78	0	-0.26	0.37	0	0	0
CHET	0.98	-0.03	0.88	0	0.08	0.55	0	0	0
FI-Hyy	0.63	-0.4	0.45	-0.81	0	0.88	0	0	0
FI-Var	0.75	-0.05	0	0	-0.21	0.66	0.97	0	0
DK-NuF/GL-NuF	0.91	-0.57	0.54	-0.1	-0.31	0.9	0	0	0
DK-ZaF/GL-ZaF	0.84	-0.45	0.69	0	-0.58	0.91	0	0	0
DK-ZaH/GL-ZaH	0.88	-0.23	0.73	0.07	-0.17	0.93	0	0	0
US-ICs	0.91	0.22	0.87	-0.48	0.2	0.78	0.7	0.93	0
US-ICh	0.87	0.23	0.87	-0.41	0.29	0.79	0.78	0.95	0
US-ICt	0.89	0.2	0.86	-0.43	0.06	0.81	0.72	0.94	0
IS-Gun	-0.51	0.71	0.42	0.97	-0.38	-0.41	0	-0.68	0
US-Rpf	0.76	-0.24	0.72	-0.7	-0.05	0.82	0.86	0.96	0
US-Prr	0.86	-0.4	0.51	-0.82	0.49	0.92	0.54	0.96	-0.85
RU-Cok	0.81	0.05	0.19	0	0.21	0.91	0.6	0	0
RU-Fyo	0.56	-0.25	0.73	-0.71	-0.25	0.9	0.72	0	-0.41
RU-Fy2	0.54	-0.52	0.55	-0.81	-0.17	0.87	0.62	0.96	-0.88
RU-Sam	0.78	0.1	0.68	-0.58	-0.19	0.61	0	0	0
RU-SkP	0.67	-0.3	0.71	0	-0.29	0.8	0.76	0.95	-0.73
YPF	0.52	-0.44	0.74	-0.7	-0.23	0.26	0	0.85	-0.46
RU-Zot	0.46	-0.31	0.46	-0.83	-0.08	0.85	0	0.93	0
CA-SCB	0.85	-0.01	0.58	-0.81	0.08	0.48	0.69	0.98	-0.85
CA-SCC	0.77	-0.05	0.62	-0.75	0.05	0.88	0.81	0.97	-0.87
SE-Fla	0.54	0	0.35	-0.7	-0.23	0.88	0	0	0
SE-Sk1	0.69	-0.26	0.27	0	0.22	0.83	0	0	0
SE-St1	0.77	-0.42	0.41	-0.78	-0.33	0.81	0	0.96	0
SJ-Adv	0.64	0.13	0.71	0	-0.07	0.96	0.4	0	0
US-Uaf	0.7	0	0.62	-0.71	0.54	0.88	0.72	0.96	0
CA-NS1	0.59	-0.19	0.37	-0.89	0.13	0.9	0	0.99	0
CA-NS2	0.19	-0.3	-0.08	-0.94	0.12	0.96	0	0.92	0
CA-NS3	0.58	-0.18	0	0	0.15	0.92	0	1	0

Table A8, Continued.

CA-NS4	-0.07	0.41	0.6	0.71	-0.46	-0.93	0	0	0
CA-NS5	0.33	-0.43	0.02	-0.97	0.26	0.91	0	0.96	0
CA-NS6	0.33	-0.55	-0.03	-0.95	0.22	0.92	0	0.93	0
CA-NS7	-0.24	0.53	-0.02	0.96	-0.04	-0.9	0	0	0

Table A9: Monthly factor loadings on the first factor for all factor analysis runs.

Site ID	ET	Precip	Temp	RH	Windspeed	SHF	GHF	Net SW	Net LW
US-An2	0.88	0.49	0.68	-0.68	0.78	0.8	0.94	0.94	-0.88
US-An1	0.88	0.3	0.69	-0.8	0.81	0.82	0	0.9	-0.88
US-An3	0.96	0.52	0.72	-0.72	0.73	0.76	0.83	0.94	-0.88
US-Atq	0.81	0.32	0.83	-0.84	-0.27	0.59	0.65	0	0
US-BZS	0.8	-0.07	0.78	-0.8	0	0.88	0.91	0.88	0
US-Bn1	0.75	-0.27	0.74	-0.91	0.37	0.92	0.93	0.97	0
US-Bn2	0.72	-0.07	0.67	-0.91	0.37	0.87	0.95	0	0
US-Bn3	0.72	-0.07	0.67	-0.91	0.37	0.87	0.95	0	0
US-BZF	0.85	-0.27	0.59	-0.9	0.69	0.41	0.91	0.99	-0.88
US-BZB	0.93	-0.19	0.69	-0.92	0.78	0.97	0.92	0.98	-0.95
CA-Man	0.91	0.46	0.64	0	-0.03	0.16	0	0	0
CHET	0.95	-0.04	0.82	0	0.48	0.72	0	0	0
FI-Hyy	0.77	-0.11	0.5	-0.79	0	0.88	0	0	0
FI-Var	0.77	0.1	0	0	-0.29	0.71	0.98	0	0
DK-NuF/GL-NuF	0.93	-0.54	0.63	0.05	-0.24	0.92	0	0	0
DK-ZaF/GL-ZaF	0.89	-0.51	0.73	0	-0.63	0.93	0	0	0
DK-ZaH/GL-ZaH	0.92	-0.07	0.82	0.39	-0.16	0.93	0	0	0
US-ICs	0.9	0.49	0.93	-0.48	0.18	0.87	0.73	0.96	0
US-ICh	0.89	0.5	0.95	-0.36	0.43	0.9	0.81	0.96	0
US-ICt	0.91	0.42	0.92	-0.42	0.02	0.88	0.77	0.94	0
IS-Gun	-0.21	0.78	0.57	0.95	-0.56	-0.71	0	-0.69	0
US-Rpf	0.76	-0.13	0.74	-0.68	-0.04	0.92	0.91	0.96	0
US-Prr	0.87	-0.36	0.53	-0.8	0.77	0.97	0.68	0.97	-0.85
RU-Cok	0.81	0.19	0.1	0	0.43	0.93	0.73	0	0
RU-Fyo	0.61	0.05	0.69	-0.7	-0.21	0.9	0.85	0	-0.31
RU-Fy2	0.65	-0.29	0.52	-0.82	-0.23	0.89	0.78	0.97	-0.87
RU-Sam	0.74	0.43	0.76	-0.6	-0.17	0.59	0	0	0
RU-SkP	0.79	-0.14	0.76	0	-0.38	0.8	0.91	0.97	-0.82
YPF	0.54	-0.17	0.86	-0.66	-0.41	0.33	0	0.89	-0.41
RU-Zot	0.59	0.09	0.62	-0.83	-0.15	0.88	0	0.98	0
CA-SCB	0.71	0.39	0.55	-0.86	0.45	0.81	0.87	0.98	-0.89
CA-SCC	0.67	0.07	0.49	-0.79	-0.14	0.96	0.95	0.99	-0.91
SE-Fla	0.48	0	0.41	-0.71	-0.46	0.9	0	0	0
SE-Sk1	0.66	-0.27	0.13	0	0.43	0.92	0	0	0
SE-St1	0.79	-0.64	0.22	-0.91	-0.16	0.9	0	0.98	0
SJ-Adv	0.61	-0.04	0.76	0	-0.47	0.98	0.43	0	0
US-Uaf	0.78	0.22	0.7	-0.67	0.73	0.92	0.84	0.97	0
CA-NS1	0.33	-0.14	0.38	-0.94	0.47	0.96	0	0.99	0
CA-NS2	0.26	-0.06	-0.21	-0.97	0.25	0.98	0	0.9	0
CA-NS3	0.64	0.02	0	0	0.43	0.95	0	0.99	0

Table A9, Continued.

CA-NS4	0.14	-0.15	-0.62	-0.67	0.82	0.93	0	0	0
CA-NS5	-0.03	-0.49	-0.18	-0.98	0.67	0.97	0	0.87	0
CA-NS6	0.13	-0.57	-0.28	-0.99	0.65	0.99	0	0.89	0
CA-NS7	-0.18	0.46	0.02	0.98	-0.22	-0.98	0	0	0

Table A10: Daily total and explained variance from multiple regressions with and without windspeed and percentage of contribution from windspeed.

Site ID	Total Variance	Explained Variance with WS	Explained Variance without WS	Windspeed Contribution (%)
ATQA	0.77	0.31	0.29	1.95
ANMB	0.9	0.79	0.79	0.11
ANSB	0.95	0.77	0.77	0
ANUB	0.38	0.3	0.3	0.53
BCBS	0.44	0	0.25	0
BCDA	0.64	0.27	0.27	0.63
BCDB	0.9	0.4	0.38	1.89
BCDC	0.9	0.4	0.38	1.89
BCFE	0.68	0.57	0.56	2.52
BCTH	0.53	0.49	0.48	2.28
CAMB	0.62	0.34	0.32	2.88
CHET	0.39	0.28	0.27	2.04
FIHY	0.73	0	0.34	0
FIVR	0.37	0.17	0.17	0.27
GLNU	0.39	0.3	0.3	0.77
GLZF	0.25	0.14	0.14	1.21
GLZH	0.27	0.16	0.16	0
ICFE	0.7	0.52	0.51	1.72
ICRI	0.67	0.44	0.43	0.9
ICTU	0.55	0.39	0.39	-0.18
ISGU	0.46	0.28	0.28	0
PFDB	0.48	0.33	0.32	2.94
PFRR	0.72	0.61	0.61	0.14
RUCO	0.56	0.23	0.23	0.36
RUFA	1.19	0.41	0.41	0.25
RUFB	0.88	0.51	0.51	0
RUSA	0.53	0.27	0.26	0.56
RUSP	0.66	0.42	0.42	0.6
RUYP	0.79	0.26	0.27	-1.39
RUZO	0.57	0.28	0.27	1.05
SEFL	0.56	0.2	0.19	1.78
SEKY	0.57	0.26	0.26	-0.35
SCCB	0.93	0.75	0.7	4.64
SCCL	0.61	0.45	0.39	10.9
STGR	0.7	0.45	0.45	0.14
SVAD	0.15	0.07	0.07	2.03
UAFS	0.59	0.41	0.41	0.17
UCIA	0.52	0.36	0.35	0.58
UCIB	0.49	0.33	0.33	0.41

Table A10, Continued.

UCIC	0.59	0.29	0.29	0
UCID	0.17	0.11	0.11	0
UCIE	0.72	0.58	0.57	0.28
UCIF	0.44	0.27	0.27	0
UCIG	0.57	0.22	0.22	0.71
Average	**0.6**	**0.37**	**0.36**	**1.12**
SD	**0.22**	**0.17**	**0.16**	**1.91**

Table A11: Weekly total and explained variance from multiple regressions with and without windspeed and percentage of contribution from windspeed.

Site ID	Total Variance	Explained Variance with WS	Explained Variance without WS	Windspeed Contribution (%)
ATQA	24.31	10.9	9.43	6.04
ANMB	29.38	24.41	24.08	1.11
ANSB	27.4	15.1	15.09	0.02
ANUB	13.59	10.82	10.8	0.14
BCBS	15.22	0	10.13	0
BCDA	21.84	13.01	13.01	0
BCDB	31.11	19.29	19.22	0.21
BCDC	31.11	19.29	19.22	0.21
BCFE	24.62	21.54	21.42	0.5
BCTH	16.63	15.91	15.76	0.87
CAMB	18	8.52	8.37	0.84
CHET	13.75	10.86	10.54	2.33
FIHY	20.77	0	10.49	0
FIVR	11.9	6.81	6.72	0.71
GLNU	13.11	11.02	11	0.21
GLZF	9.97	6.8	6.72	0.8
GLZH	10.54	7.1	7.1	0.03
ICFE	25.34	20.19	19.91	1.11
ICRI	24.05	17.38	17.13	1.06
ICTU	20.22	16.1	16.24	-0.7
ISGU	9.1	5.82	5.63	2.15
PFDB	15.52	10.95	10.57	2.48
PFRR	22.22	18.84	18.76	0.38
RUCO	22.54	11.53	11.53	0
RUFA	32.72	10.88	10.87	0.03
RUFB	24.73	15.13	15.11	0.07
RUSA	21.18	10.7	10.69	0.02
RUSP	25.19	20.19	20.17	0.1
RUYP	19.24	13.25	12.93	1.69
RUZO	19.85	6.27	6.16	0.54
SEFL	17.77	4.88	4.75	0.76
SEKY	16.81	5.26	5.35	-0.5
SCCB	27.67	21.82	21.35	1.7
SCCL	23.85	16.96	16.39	2.4
STGR	25.21	14.25	14.24	0.04
SVAD	6.53	3.94	3.68	3.89
UAFS	22.97	14.99	14.98	0.01
UCIA	12.2	9.41	9.4	0.04
UCIB	16.66	9.76	9.7	0.35

Table A11, Continued.

UCIC	18.58	12.29	12.29	0
UCID	5.74	3.72	3.68	0.71
UCIE	23.38	18.25	18.11	0.59
UCIF	12.74	8.55	8.53	0.19
UCIG	17.48	5.44	5.38	0.35
Average	**19.61**	**12.57**	**12.33**	**0.8**
SD	**6.67**	**5.5**	**5.37**	**1.23**